A Wavelet-based Approach for Truncating Pulse-like Records

Vicky Dimakopoulou (vdimak@central.ntua.gr)
National Technical University of Athens: Ethniko Metsobio Polytechneio https://orcid.org/0000-0002-6396-7425

Michalis Fragiadakis
National Technical University of Athens: Ethniko Metsobio Polytechneio https://orcid.org/0000-0002-0698-822X

Ioannis Taflampas
National Technical University of Athens: Ethniko Metsobio Polytechneio

Research Article

Keywords: Record truncation, effective duration, predominant pulse, pulse-like, pulse index, near-field

Posted Date: February 9th, 2021

DOI: https://doi.org/10.21203/rs.3.rs-214132/v1

Version of Record: A version of this preprint was published at Bulletin of Earthquake Engineering on October 7th, 2021. See the published version at https://doi.org/10.1007/s10518-021-01224-8.

A wavelet-based approach for truncating pulse-like records

Vicky Dimakopoulou[1], Michalis Fragiadakis, Ioannis Taflampas
School of Civil Engineering, National Technical University, Athens, Greece

Abstract

The seismic performance assessment of structures using truncated pulse-like ground motion records is discussed. It is shown that it is possible to truncate pulse-like signals using a novel wavelet-based definition that identifies the duration of the predominant velocity pulse. The truncated time history can efficiently reproduce the increased seismic demand that near-field records typically produce. Substituting the original ground motion with the truncated signal, significantly accelerates structural analysis and design. The truncated signal is the part of the original accelerogram that coincides with the duration of the predominant pulse, which is identified using a wavelet-based procedure, previously proposed by the authors. Elastic and inelastic response spectra and nonlinear time history analyses for SDOF (single-degree-of-freedom) systems are first studied. Subsequently a nine-storey steel frame is examined in order to demonstrate the performance of the proposed approach on a multiple-degree-of-freedom system. The proposed approach is found very efficient for pulse-like ground motions, while it is also sufficient for many records that are not characterized as such.

KEY WORDS

Record truncation; effective duration; predominant pulse; pulse-like; pulse index; near-field.

INTRODUCTION

Replacing an acceleration time history with an equivalent, "truncated", signal has many benefits in terms of accelerating the seismic performance assessment and also for understanding structural response. Although this is a very appealing approach, experience has shown that there is no silver bullet to the problem. It is practically impossible to have a record truncation algorithm that is efficient and accurate for all ground motions and all structural systems possible. However, if the problem is narrowed down to the case of pulse-like ground motions, it is possible to achieve an efficient truncation using a novel wavelet-based

[1]E-mail: vdimak@central.ntua.gr, https://orcid.org/0000-0002-6396-7425

definition for the record effective duration. The effective duration is calculated first fitting a wavelet on the ground motion and then truncating the record to the time interval that corresponds to the fitted wavelet.

The problem of record truncation is paired with the definition of "effective" record duration. Once the record effective duration is known, the signal can be truncated to the corresponding time interval. However, existing duration definitions such as "bracketed" and "uniform" duration (e.g. Bolt 1973, Bommer & Martinez-Pereira 1996, Bommer & Martinez-Pereira 2000, Riddell 2007, Taflampas *et al.* 2008), do not permit an efficient signal truncation that can substitute the original signal for time history simulations. This is because the intervals defined using those duration definitions omit important information of the original signal. Furthermore, the truncated signal does not have zero, or close to zero, acceleration values at their beginning and end. This problem cannot be easily fixed with baseline correction algorithms.

One of the early efforts for record truncation was that of Srivastav and Nau (1998) who studied the influence of truncated earthquake records on the response of long-period structures. They recommend truncating the earthquake record at a small value of acceleration in order to reduce the error. However, most efforts are based on Arias intensity. For example, Jin *et al.* (2020) proposed the use of Arias intensity in order to study arch dams, while artificial intelligence approaches have been also proposed, e.g., Khaloo *et al.* (2006).

The scope of this study is to adopt the wavelet-based duration definition proposed by Repapis *et al.* (2020) in order to truncate the acceleration time history and obtain a simpler and shorter signal. The paper shows that this practice can efficiently accelerate the simulation time with minor loss of accuracy. The efficiency of the proposed truncation approach depends on the pulse content of the record, which can be quantified with the aid of a pulse index. The approach proposed is quite efficient in the case of pulse-like records, such as those recorded in the case of near-field ground motions with forward directivity. These signals are characterised by strong, coherent, long period pulses that are found mainly in the strike normal direction. The effect of significant velocity pulse on the structural response, has been highlighted by several studies, i.e. Bertero and Mahin (1978), Chopra and Chintanapakdee (2001), Spyrakos *et al.* (2008).

METHODOLOGY

Figure 1 shows two characteristic pulse-like ground motion records and the corresponding significant pulses. The pulses have been identified using the methodology proposed by Mimoglou *et al.* (2014), i.e., appropriately fitting a wavelet on the signal. The plot on the right shows the cumulative energy flux and the time limits that correspond to the proposed "wavelet-based duration" (black dashed lines). The plots also show the 5% and the 95% of the record energy flux (dashed grey lines), which was proposed by Trifunac and Bray (1975) as a measure of the record "significant duration". Clearly, the two definitions of record duration differ considerably (Figure 1a).

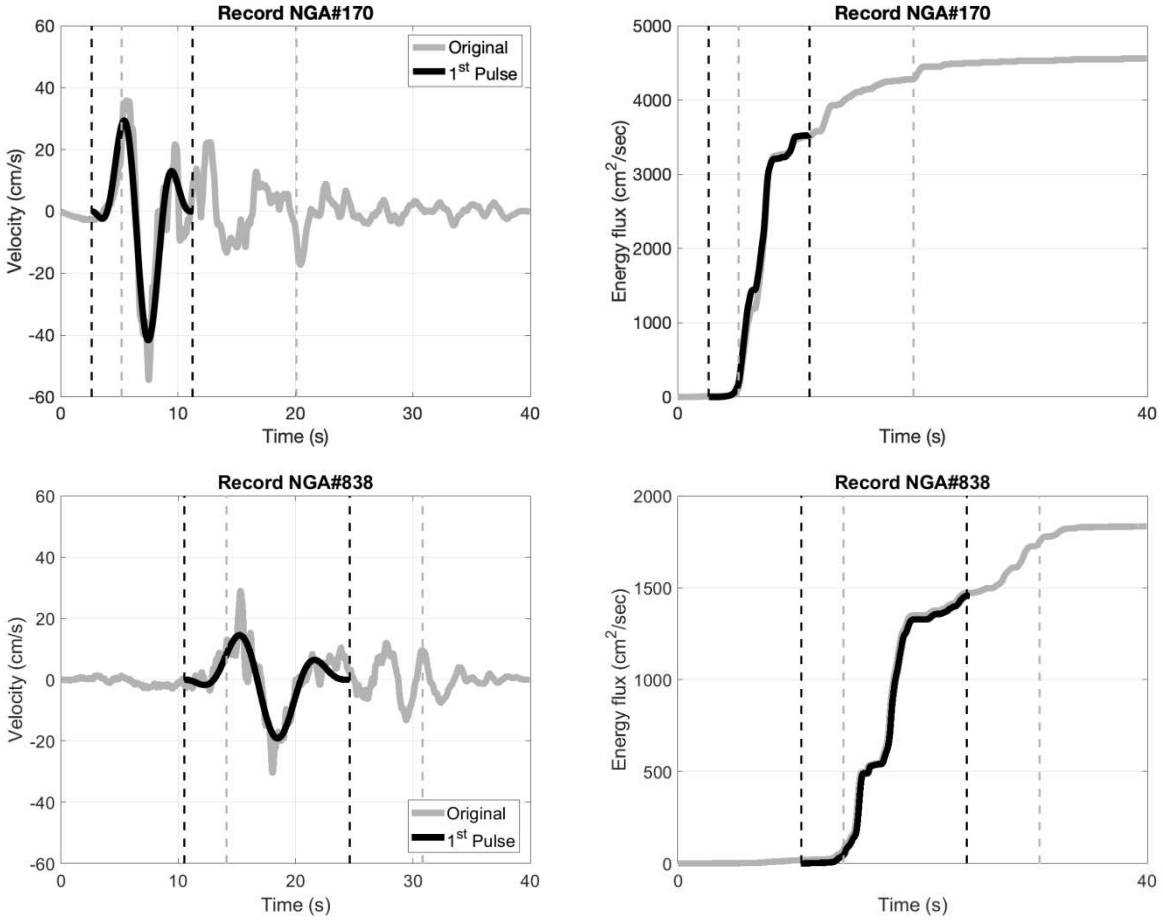

(a) (b)

Figure 1: (a) Velocity time history showing the total, the proposed wavelet-based and the significant duration definition, (b) Energy flux (records NGA #170 and NGA #838).

In order to calculate the record duration, we first extract the predominant pulse. According to Mimoglou *et al.* (2014), the extraction is based on optimally fitting the Mavroeidis and Papageorgiou (2003) wavelet on the signal. This is a versatile wavelet, suitable to represent different duration levels, since it includes a parameter that is explicitly associated with the

number of pulse cycles. A further advantage of this wavelet is that it is defined as the product of a sinusoidal periodic function and a bell-shaped envelope.

The Mavroeidis and Papageorgiou (2003) wavelet depends on four parameters that control the frequency (T_p), the amplitude (A), the number of cycles (γ) and the polarity (φ) of the signal. The frequency is obtained as the period value that the product of velocity and displacement spectra becomes maximum. An exhaustive search algorithm is then adopted in order to identify the other three parameters; the search is narrowed to two parameters since the amplitude and the number of cycles are related by the expression (Taflampas *et al.* 2008):

$$CAD = \frac{\gamma A T_p}{\pi} \tag{1}$$

where CAD is the cumulative absolute displacement, obtained as the integral of the absolute value of ground velocity. The wavelet parameters that have the best cross-correlation value with the original signal define the most suitable wavelet model of the record predominant pulse. Once the wavelet is fitted on the ground motion, e.g., see Figure 1a, the wavelet-based effective duration of the signal is defined by the time boundaries of the fitted pulse.

The truncated signal is the part of the original record contained in the time boundaries of the wavelet that represents the predominant pulse (Figure 1a black vertical lines). Therefore, the truncated signal contains all the information, including the high frequency information, of the original ground motion. Moreover, according to Figure 1b, the ends of the proposed duration definition appear at points where the graph of the energy flux shows a horizontal step with zero first gradient. Therefore, there is no significant baseline offset at the beginning and the end of the truncated duration. This is not the case with other duration definitions, e.g. the "significant duration" definition that use the arbitrary limits of 5 to 95% of the total energy flux in order to truncate the ground motion.

Thanks to the proposed wavelet fitting, the time boundaries identified, ensure that the truncated signal starts and ends at an acceleration value close to zero, similarly to the case of recorded acceleration time histories. Therefore, the limits of the envelope can be considered as boundary tapers that attenuate the harmonic function and smooth the baseline of the cut-off instants. This can be better understood looking at Figure 2, where the acceleration and velocity of six truncated signals are shown. The time histories approach smoothly the zero acceleration and velocity line which allows to use them for structural response history simulations without the need for further processing.

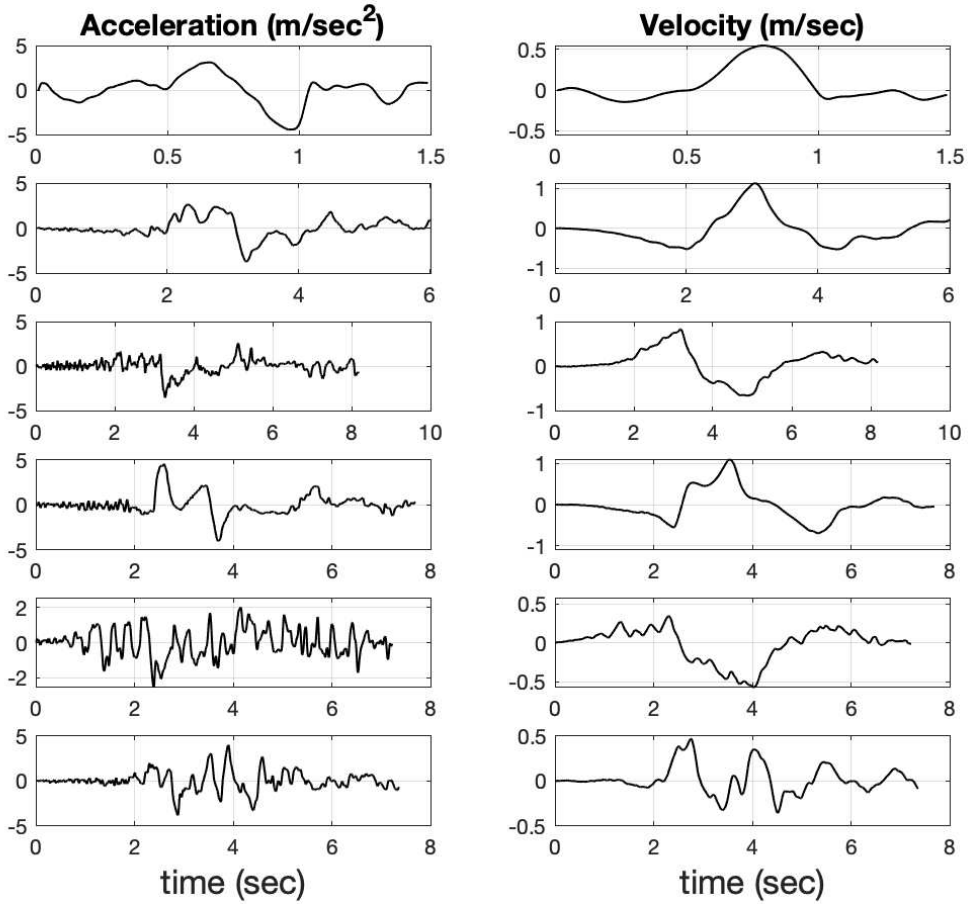

Figure 2: Acceleration and velocity time histories of truncated signals.

Forty-eight (48) pulse-like records (see next section), obtained from the PEER-NGA2-West database, are used throughout this work, unless otherwise specified. Figure 3 shows the proposed truncated duration definition on the energy flux diagrams (Husid 1969, Arias 1970, Sarma 1971) for twelve of the examined records. The records shown correspond to ground motions of increasing pulse period, T_p. The black line corresponds to the wavelet-based truncated record, shifted in time so that the pulse of the original and of the truncated records coincide. It is seen that in all cases, the proposed duration coincides with the abrupt energy flux release, associated with the near-field effects. Most importantly, for the majority of the examined excitations, the record duration has been significantly reduced, on average by 80%.

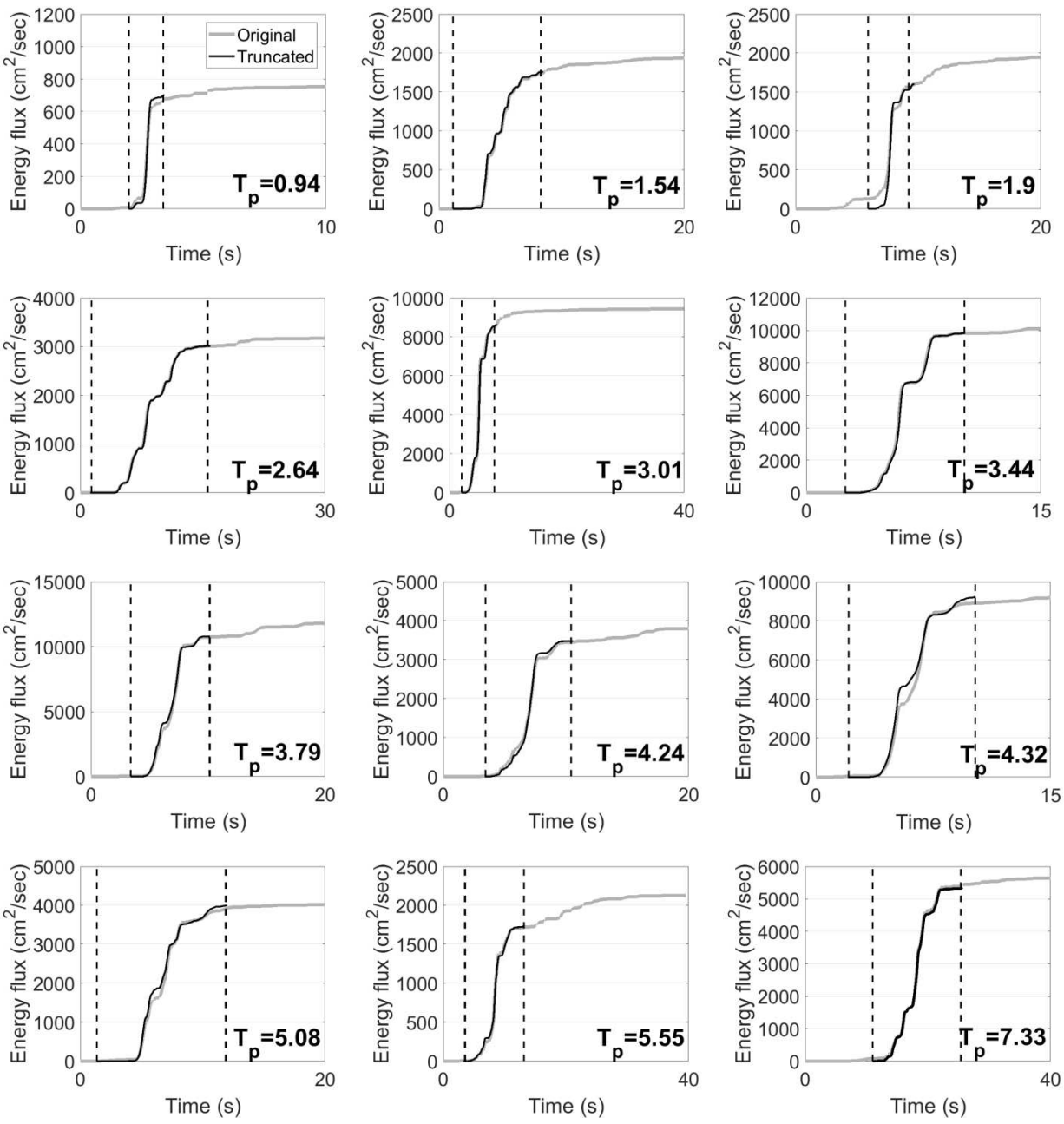

Figure 3: Energy flux and proposed wavelet-based duration for twelve ground motions.

Figure 4 compares the constant ductility displacement spectra of the ground motions of Figure 3, using elastoplastic single-degree-of-freedom (SDOF) oscillators with a constant ductility factor equal to 6. Both original and truncated signals show maximum displacement demand at period values close to the predominant period of the pulse. Clearly, high accuracy has been obtained using the truncated records instead of the original acceleration histories. Furthermore, Figure 5 shows for the set of 48 ground motions, the mean constant ductility displacement spectra for ductility factors equal to μ=2 and μ=6 (Figure 5a). Figure 5b shows also the corresponding coefficient of variation (CoV) as function of the period of the SDOF

system. The agreement on the mean demand is remarkable for both ductility levels values considered, i.e. perfect agreement is seen for the two inelastic examined cases (μ=2, μ=6) case, while, most importantly, the dispersion is practically not affected when the truncated signal (Figure 5b) is adopted. This implies that the proposed wavelet-based truncation approach is accurate and robust for elastoplastic SDOF systems.

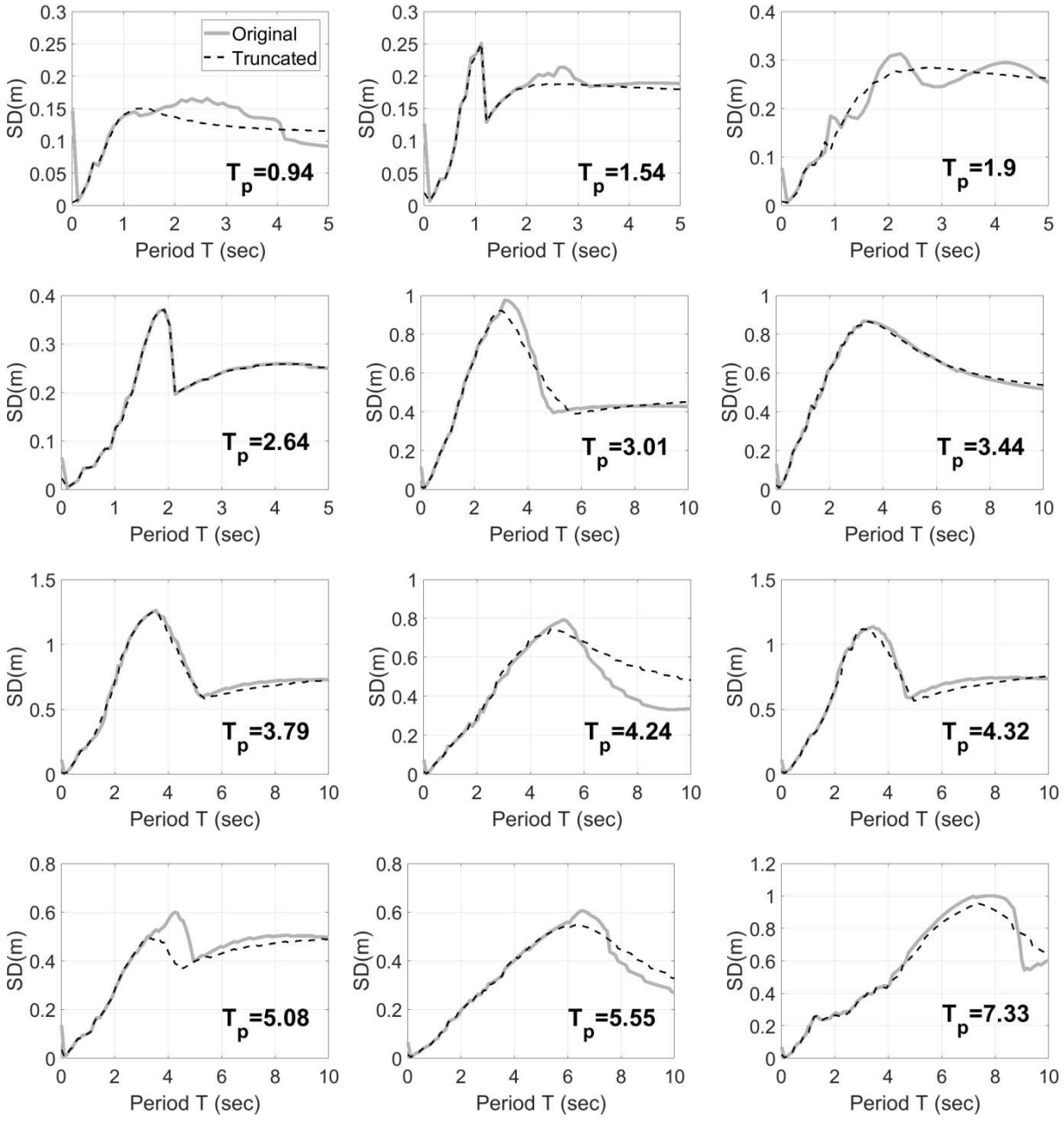

Figure 4: Displacement spectra with constant ductility μ=6.

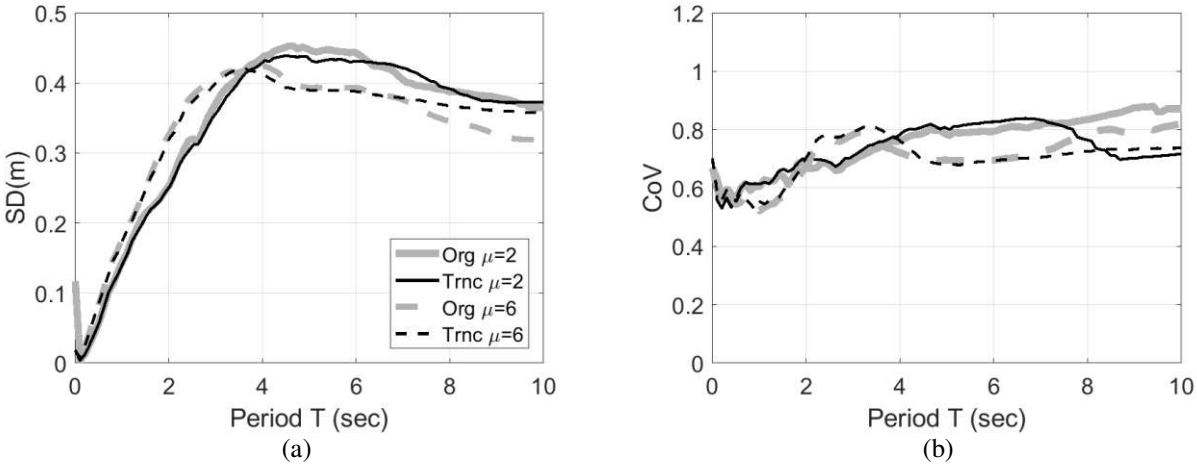

Figure 5: (a) Mean inelastic displacement spectra, (b) coefficient of variation of inelastic displacement spectra, calculated for constant ductility μ factor equal to μ=2 (solid line) and μ=6 (dashed line).

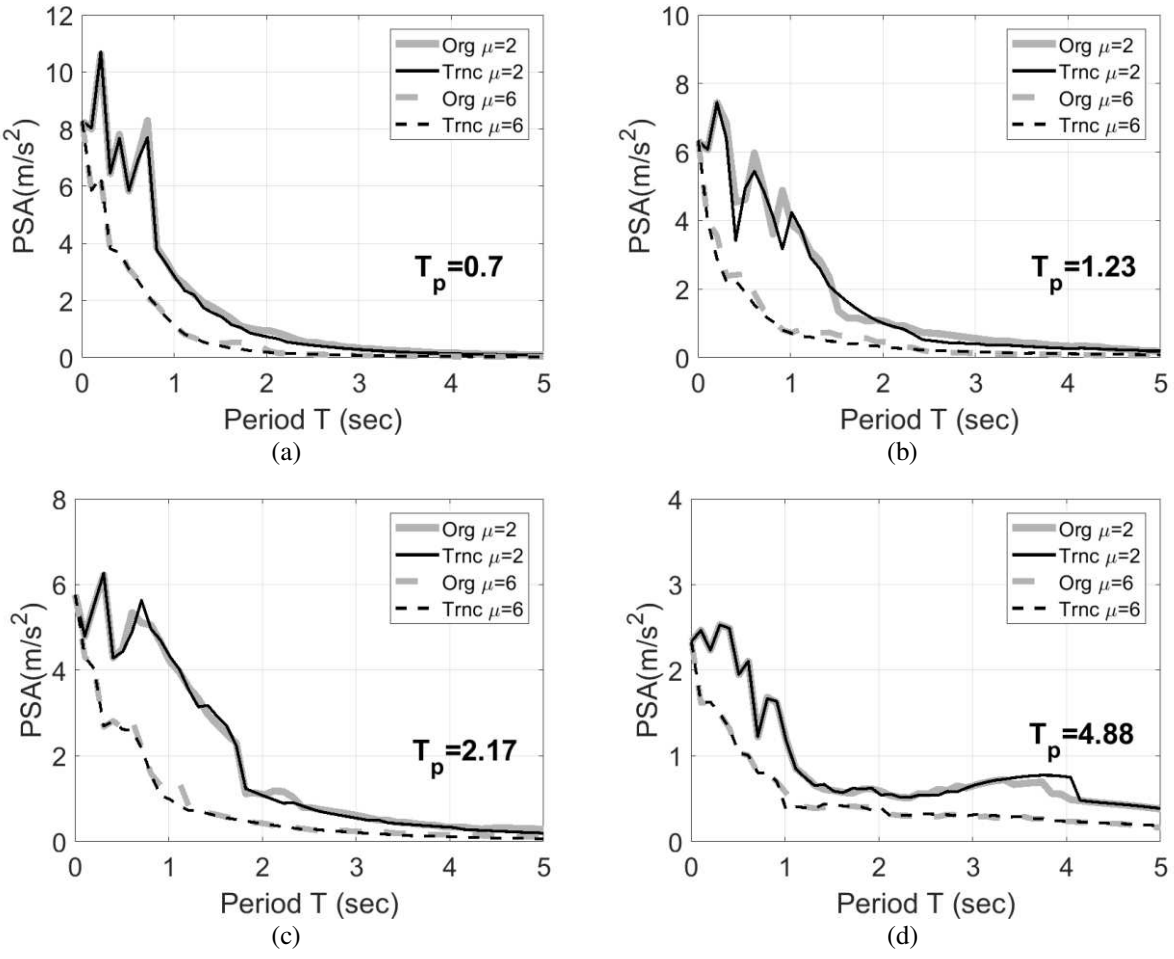

Figure 6: Constant ductility acceleration spectra (μ=2, 6): (a) NGA#568, (b) NGA#1119, (c) NGA#1013, (d) NGA#1161.

The agreement between the original and the wavelet-based truncated records is further studied using the constant ductility, μ, acceleration spectra of Figure 6. In acceleration spectra the maximum demand occurs at period values slightly less than the $0.5T_p$, as opposed to

displacement spectra (Figure 4) where the maximum occurs at period values close to T_p. Figure 6 shows the 5%-damped constant ductility acceleration spectra for four ground motions, with T_p = 0.7, 1.23, 2.17 and 4.88 sec, respectively, and ductility factors equal to μ=2 and μ=6. As in the case of displacement spectra, the elastoplastic constant ductility spectra, of the original and the truncated ground motion perfectly coincide regardless of the period value and the level of inelastic demand.

GROUND MOTION RECORDS

A set of 48 pulse-like ground motion records, included in the PEER-NGA2-West database, have been selected for our work. The properties of the ground motions are summarized in the Appendix. The excitations were recorded on different soil types and distances from the rupture plane and have different values of predominant pulse periods. Moreover, the selected ground motion sample contains records with strong directivity, mainly in the fault-normal direction (e.g., Loma Prieta), or records where both the fault-normal and the fault-parallel components show prominent directivity effects (e.g., Erzincan-Turkey).

CORRELATION WITH PULSE INDEX

The proposed wavelet-based truncation, in principle, applies to pulse-like ground motions. When pulse-type records are considered, the seismic energy is suddenly released from the fault producing few strong ground motion cycles. In this case the seismic demand obtained with the truncated and the original ground motions is expected to be close. However, often the proposed approach gives sufficiently accurate results also for records that have been a priori classified as non pulse-like. It is, therefore, very useful to have a metric that can be used to determine, prior any analysis, if the proposed truncation can be used to substitute the original signal. An obvious metric suitable for this purpose is a “pulse index” such as the one proposed by Baker (2007) and/or Kardoutsou *et al.* (2017).

Kardoutsou *et al.* (2017), proposed as a pulse index (*PI*) the cross-correlation of the original signal and the extracted wavelet. This work was also based on fitting the Mavroeidis and Papageorgiou wavelet, as discussed in Mimoglou *et al.* (2014). The authors recommend that records with *PI* less than 0.55 are non-pulse like, while when *PI*>0.65 the record is definitely pulse-like. Records with intermediate values, i.e., 0.55<*PI*<0.65, are characterized as ambiguous. Figure 7 compares the ratio of peak displacement demand of the original and the wavelet-based truncated time-history versus the Pulse Index (*PI*). The comparison is based on

the record set of FEMA P-695 (2009). A different and well-known record database is adopted for this comparison in order to use ground motions that are completely different from those used in their previous studies of the authors (Kardoutsou *et al.* 2017, Mimoglou *et al.* 2014). The ground motion set of FEMA P-695 (2009) consists of 44 far-field records, 28 near-field records characterized as "pulse-type" and 26 near-field records characterized as "non pulse-type". The far-field set includes earthquakes of large magnitude (M_w>6.5), recorded on soil types C and D according to the NEHRP classification. The pulse-type set contains records, with varying pulse periods, corresponding to events of magnitude between 6.5 and 7.6. These records present strong directivity effects in the fault-normal/and or the fault parallel direction.

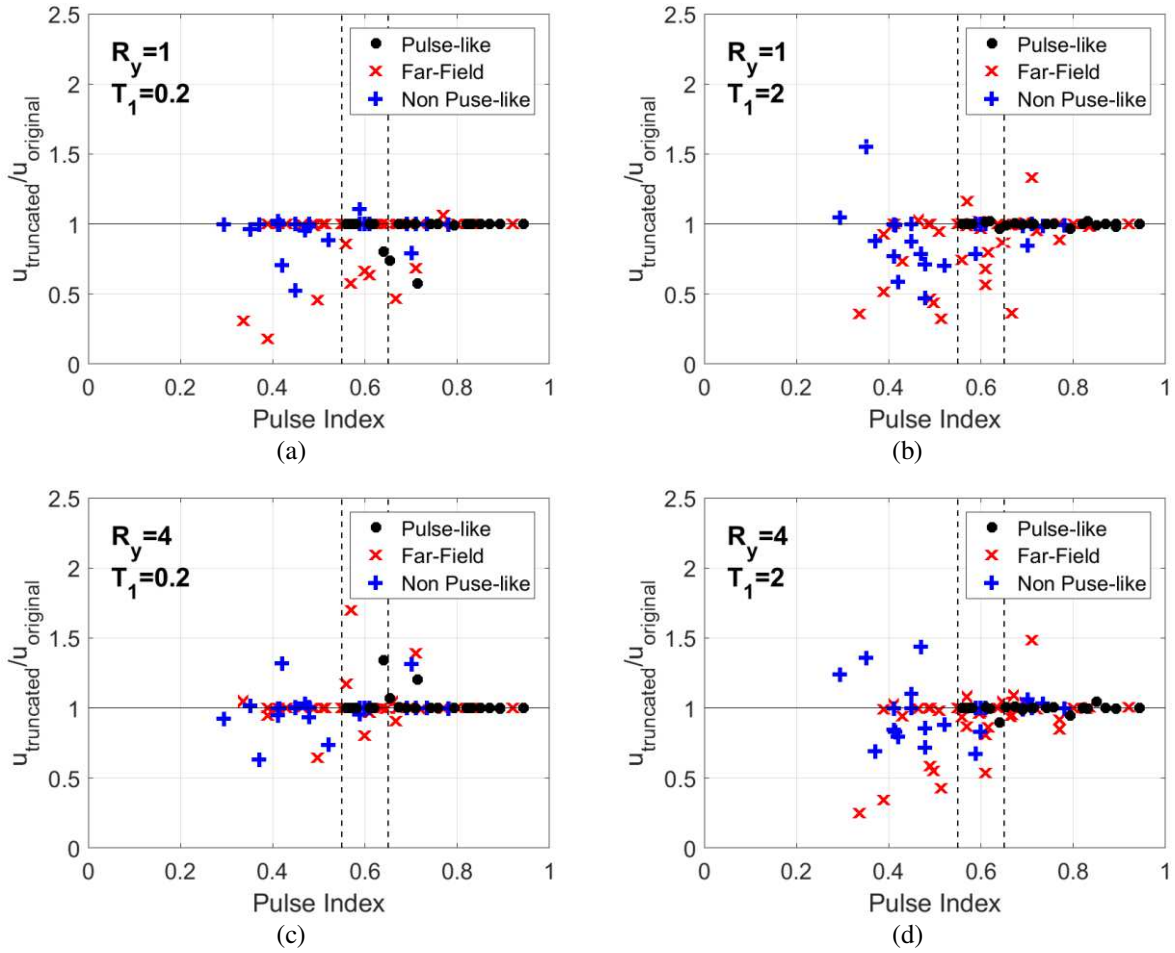

Figure 7: Ratio of the maximum top displacement of elastoplastic SDOF systems computed for the original and truncated record versus the corresponding pulse index for elastoplastic systems with: (a) R_y=1, T_1=0.2sec, (b) R_y=1, T_1=2sec, (c) R_y=4, T_1=0.2sec, and (d) R_y=4, T_1=2sec.

The ratio of displacements shown in Figure 7 is computed for elastoplastic SDOF systems with natural periods T_1 equal to 0.2 and 2 sec and constant R_y factors equal to 1 and 4. R_y is the strength reduction factor, equal to the ratio of the ζ%-damped spectral acceleration demand S_a (T_1,ζ) over the corresponding yield acceleration. The horizontal axis in Figure 7

shows the *PI* value of every record and the vertical axis shows the ratio of SDOF displacement demand of the truncated over the original signal $u_{truncated}/u_{original}$. For the "pulse-like" ground motions, it is seen that all records have a *PI* value above 0.60, while nearly perfect agreement between the truncated and the original record has been achieved, i.e. almost all points lie on a horizontal line with $u_{truncated}/u_{original}$ equal to one. However, for "non-pulse like" records, the index clearly receives small values, as low as $PI<0.3$, while the majority of the records have *PIs* below 0.65; thus for non-pulse records there is loss of accuracy that may reach 50%. Nevertheless, even in this case, there are simulations where the prediction of the truncated record is close to that of the original signal. Finally, for the "far-field" ground motions the *PI* index varies between 0.3 and 0.9, with a median *PI* value about equal to 0.6. Relatively good accuracy is also achieved for this set, despite the large inelastic demand due to the $R_y=4$ assumption. Overall, for the $T_1=0.2$ sec and $T_1=2$ sec cases, the predictions are considered better in the former case. Another point of interest is that there seems to be a bias towards underestimating the demand when the truncated motion is adopted. This is expected since the truncated record is a "simplified" version of the original record and hence contains less energy. However, there are some simulations where the demand is, slightly, overestimated. This unexpected behavior can be attributed to a distortion in the baseline which in turn affects the displacements estimate.

Based on the discussion above, a *PI* index, e.g., that of Kardoutsou *et al.* (2017), can be used to identify if the record is pulse-like and hence if the proposed wavelet-based truncation is applicable. Large *PI* values, above 0.6, indicate that the substitution of the original ground motion will be successful, while smaller values imply that attention is required when truncating the signal.

NUMERICAL INVESTIGATION

Degrading Single-Degree-of-Freedom (SDOF) oscillators

Three degrading single-degree-of-freedom (SDOF) oscillators are studied in order to further investigate the accuracy and the efficiency of the proposed truncation approach. The oscillators have in-cycle degradation (i.e., degradation of the monotonic envelope) as shown in Figure 8. Compared to the elastoplastic systems already examined, these are simple SDOF systems but more realistic since real-world systems are not elastoplastic with infinite capacity. The importance of studying degrading systems in the case of pulse-like ground motions is further discussed in Dimakopoulou *et al.* (2013).

The oscillator of Figure 8a is considered representative of non-ductile systems commonly found in Southern Europe; it will be used as our reference degrading oscillator. Using the parameterization of Figure 8a, the properties of the backbone are: a_h=5%, a_c=-50%, μ_c=2 and r=20%. A "brittle" and a "ductile" oscillator are also considered. The backbone curves of all three oscillators are shown in Figure 8b and their properties are summarized in Table 1. The cyclic response of all examined systems is based on the "hysteretic material" available in the material library of the OpenSees software (McKenna and Fenves, 2001). The force and displacement pinching parameters of the model are set equal to a moderate value.

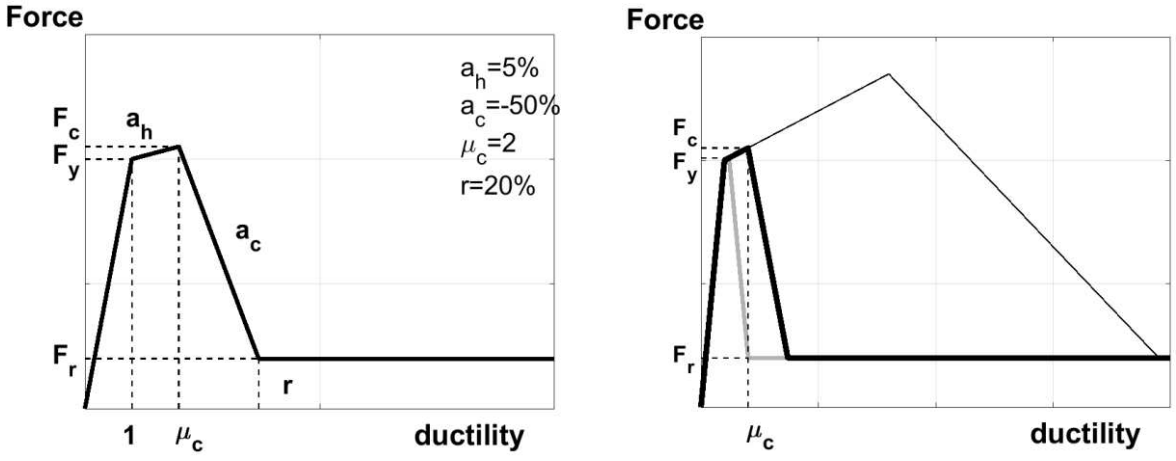

Figure 8: (a) Reference oscillator, (b) brittle oscillator (light grey line), ductile oscillator (black thin line) and reference oscillator (black line).

Table 1: SDOF oscillator parameters

Oscillator Type	a_h	a_c	μ_c	r
Reference	5%	-50%	2	20%
Ductile	5%	-10%	8	20%
Brittle	5%	-100%	1.2	20%

In order to investigate the response of the SDOF systems, plots of the oscillator period versus the inelastic displacement ratio C_R are shown. The ratio C_R is calculated as $C_R=u_m/u_{el}=\mu/R_y$. In C_R, the subscript "R" denotes that C_R has been calculated keeping constant the strength reduction factor R_y. For a constant R_y value, C_R is linearly related to the maximum ductility demand μ and hence it is a good seismic demand indicator (Ruiz-García and Miranda 2007). Furthermore, as discussed in Dimakopoulou *et al.* (2013), the plots have been normalized as function of the predominant pulse period, T_p. This is better explained in Figure 9; in Figure 9a the curves are plotted against the period T_1 as opposed to Figure 9b where the period axis has been normalized with the pulse period T_p. Plotting T_1/T_p shifts the spectral values towards the vicinity of T_p. Therefore, normalizing with T_p, reduces the dispersion, which indicates that the ratio T_1/T_p is better correlated with the demand.

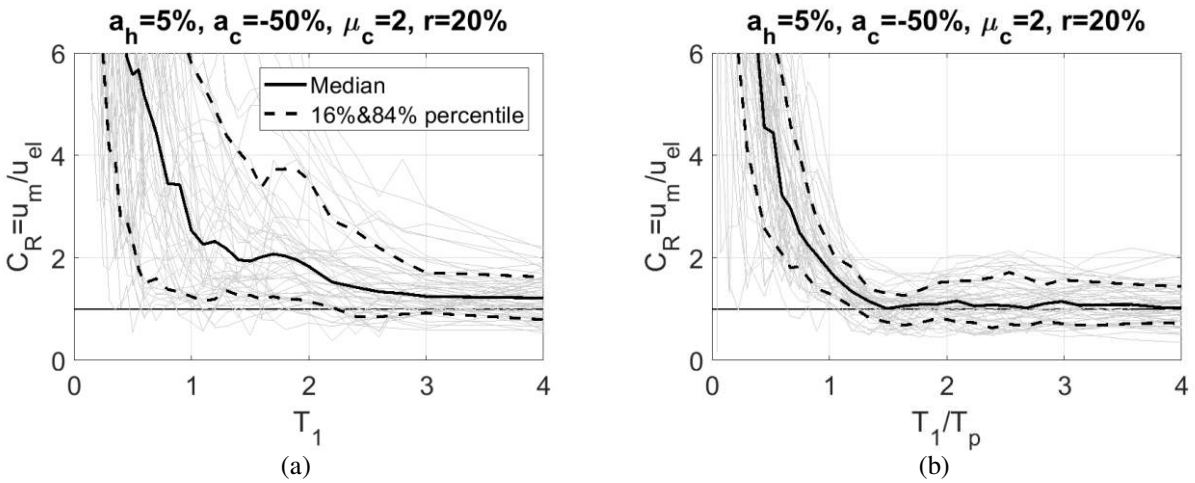

(a) (b)

Figure 9: Reference oscillator (R_y=6) under original ground motions: C_R ratio values versus (a) oscillator period T_1, (b) oscillator period normalized with the pulse period T_1/T_p.

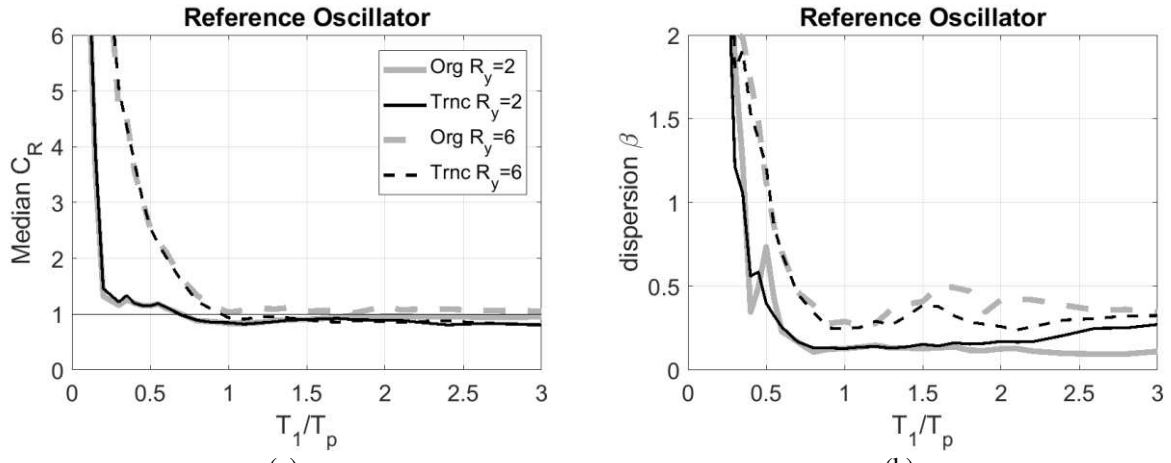

(a) (b)

Figure 10: (a) Median C_R of the reference degrading SDOF oscillator subjected to the original ground motion and the corresponding truncated signal for R_y=2 and R_y=6, (b) dispersion β of C_R, calculated for R_y=2 and R_y=6.

Figure 10, Figure 11 and Figure 12 compare the C_R demand as function of the ratio T_1/T_p for systems with strength reduction factor equal to R_y=2 and 6. The median C_R demand is shown on the left (Figure 10a, Figure 11a and Figure 12a), while the corresponding dispersion is provided. The dispersion has been calculated as $\beta = (Prc_{84\%} - Prc_{16\%})/2$. For the reference oscillator (Figure 10), the inelastic displacement ratio decreases exponentially as the normalized period T_1/T_p increases, while, for both R_y values shown, the response predicted by the truncated signal is practically identical to that of the original record. Good accuracy is also observed for the brittle (Figure 11) and the ductile oscillators (Figure 12), although the median response is different for each of the oscillators considered. It is also shown that the R_y value controls the slope of the descending branch as the median curves approach the horizontal line at C_R=1, which corresponds to the equal displacement rule.

Close agreement is also seen in the dispersion plots. This means that despite the record-to-record variability, the truncated signal can adequately substitute the original ground motion throughout the period range and regardless the level of R_y and the oscillator properties.

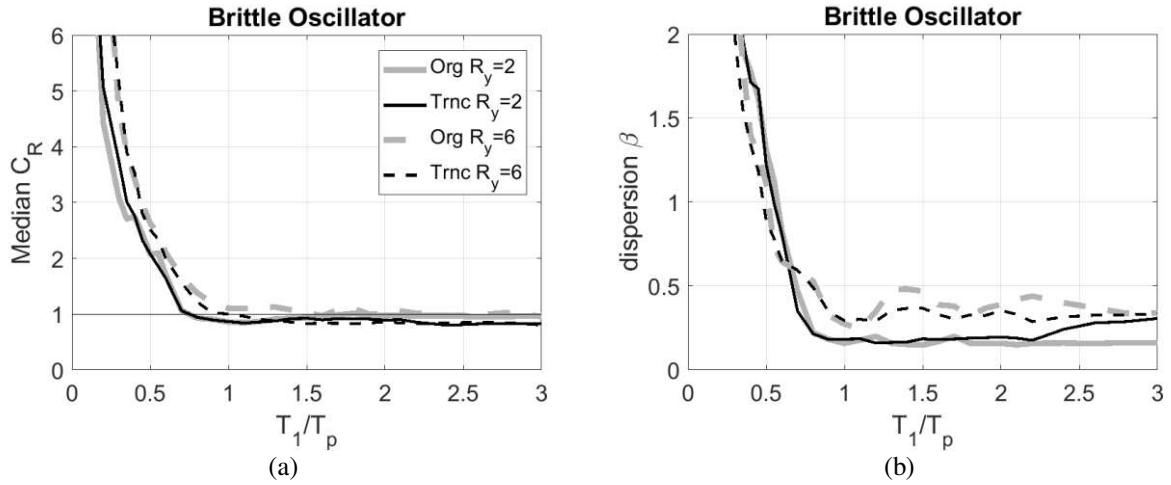

Figure 11: (a) Median C_R of the brittle oscillator subjected to the original ground motion and the corresponding truncated signal for R_y=2 and R_y=6, (b) dispersion β of C_R, calculated for R_y=2 and R_y=6.

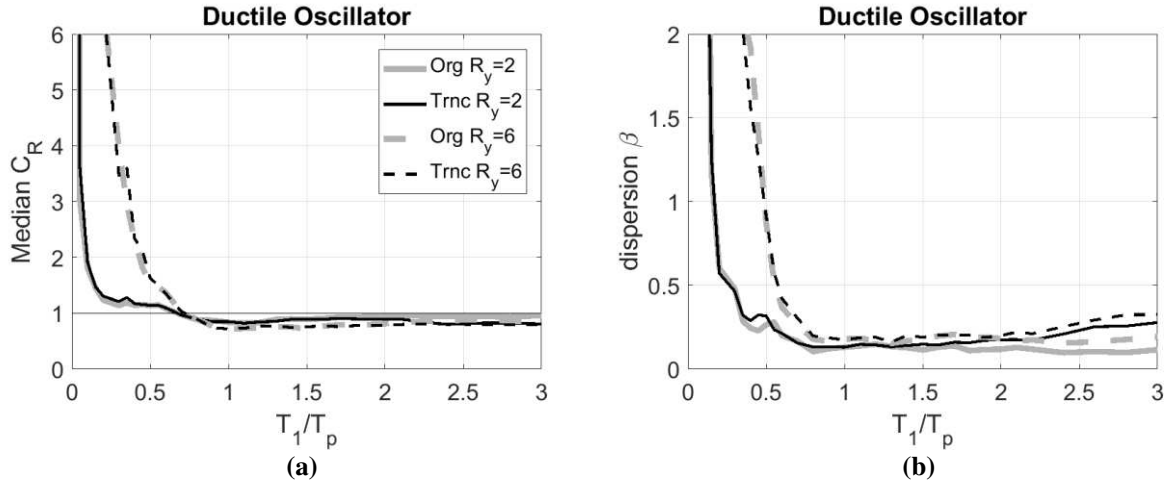

Figure 12: Median C_R of the ductile oscillator subjected to the original ground motion and the corresponding truncated signal for R_y=2 and R_y=6, (b) dispersion β of C_R, calculated for R_y=2 and R_y=6.

Nine-storey steel frame

The efficiency of the proposed record truncation approach is also studied using a nine-storey steel moment-resisting frame. The well-know LA9 frame is used as a testbed multi-degree-of-freedom (MDOF) structure. The building consists of five bays and a hinge-storey basement. The gravity loads and the mass of the internal gravity-resisting frames are placed on a leaning column, which does not contribute to the lateral stiffness. The fundamental period of the frame was found equal to T_1=2.35 sec and the mass modal participation of the first mode amounts to 84% of the total mass. Thus, the frame is essentially dominated by the

first mode, while higher modes may also contribute to the response. The cross-sections and more details about the building design can be found in Gupta & Krawinkler (1999).

A centreline model is adopted using the OpenSees platform (McKenna and Fenves, 2001). The model account explicitly for the geometric nonlinearities in the form of $P-\Delta$ effects. The columns are assumed linear-elastic, while a quadrilinear model is adopted for the beam-column connections. The backbone of the moment-rotation relationship is based on a model that follows the palettization of the force-deformation relationship of the degrading SDOF systems (Figure 8). More specifically, the moment-rotation relationship of all beam-column connections have properties equal to: a_h=10%, a_c=-50%, μ_c=3 and r=50%.

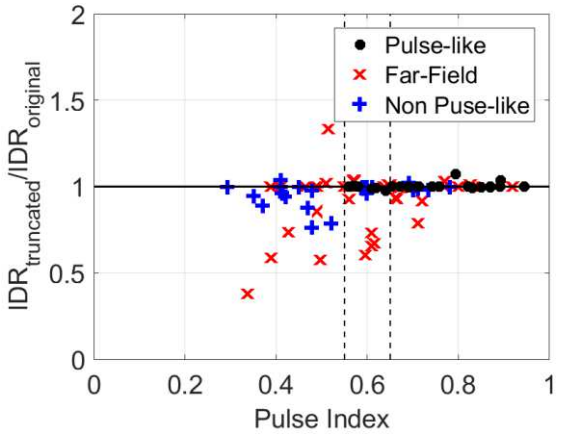

Figure 13: Ratio of the maximum interstorey drift for the 9-storey steel moment frame versus the calculated cross correlation.

Figure 13 shows a comparison similar to that of Figure 7, where the ratio of peak interstorey drift is plotted against the pulse indicator (*PI*) for the three record sets of FEMA P-695. The difference in the maximum peak interstorey drift demand between the original and the truncated records is small for ground motions with a pulse indicator *PI* above the 0.65 threshold. This observation holds even for records that belong to the far-field set. The largest differences are again found for the far-field records (red crosses), but even for *PI*<0.55 the differences do not seem to exceed on average 18%. Overall, for the building examined, the scatter in the computed drift values is significantly decreased as *PI* increases, regardless of the classification of the ground motion record. This indicates the efficiency of the proposed wavelet-based approach for truncating a ground motion record and also the potential on the proposed pulse index *PI* metric to quickly assess using the efficiency of the proposed wavelet-based truncation.

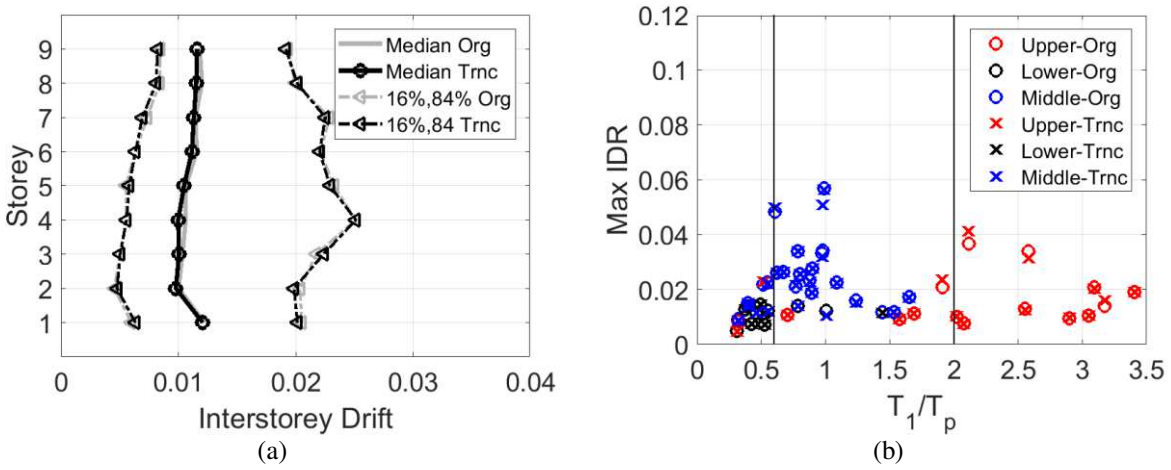

Figure 14: (a) Profile of the median and the 16 and 84% percentiles drift demand for the 48 pulse-type ground motions; (b) Maximum interstorey drift obtained using the original and the truncated records versus the T_1/T_p ratio

The LA9 steel frame was subjected to the 48 pulse-like records. Figure 14a presents the median peak interstorey drift demand and the corresponding 16% and 84% percentile curves of the interstorey drift demand. Excellent agreement for all the stories has been achieved along the height of the frame. Furthermore, the effect of record-to-record variability on the maximum interstorey drift demand is studied in Figure 14b. Although minor differences are seen for individual records, for the majority of ground motions the drift estimates of the original and the truncated signal practically coincide. Figure 14b deserves further attention. A different marker colour has been adopted depending on the storey that the maximum interstorey drift occurred. Overall, the seismic response computed for the truncated signals, follows the same pattern observed for the original records while for most cases the maximum drift demand occurs at the same level. Since the structure studied is sensitive to the first mode, the larger demand is due to records with $T_1/T_p \leq 1$. Furthermore, for these records, the peak drift appears at the middle stories (stories 4, 5 and 6).

Our findings are in agreement with Baker and Cornel (2008) who discuss the effect of pulse period on the seismic behaviour of MDOF systems. They investigated the effect of the pulse on the higher modes of excitation through MDOF structures sensitive to second mode excitation and suggested that the ratio T_1/T_p is indicative of the level at which the peak displacement occurs; short period records excite higher modes, while for records with long period pulses the maximum response is expected at the low stories, indicating that first mode response governs the peak displacements of the building. They proposed the thresholds, $T_1/T_p<0.5$ and $T_1/T_p>2$ that are also shown as vertical dashed lines in Figure 14b. According to Figure 14, for records with short period pulses, $T_1/T_p>2$ the higher modes of vibration are

excited and the maximum interstorey drift is located at the upper stories (stories 7, 8 and 9). On the other hand, for records with $T_1/T_p<1$, the maximum drift demand is observed at lower stories, indicating that the response is first mode dominated.

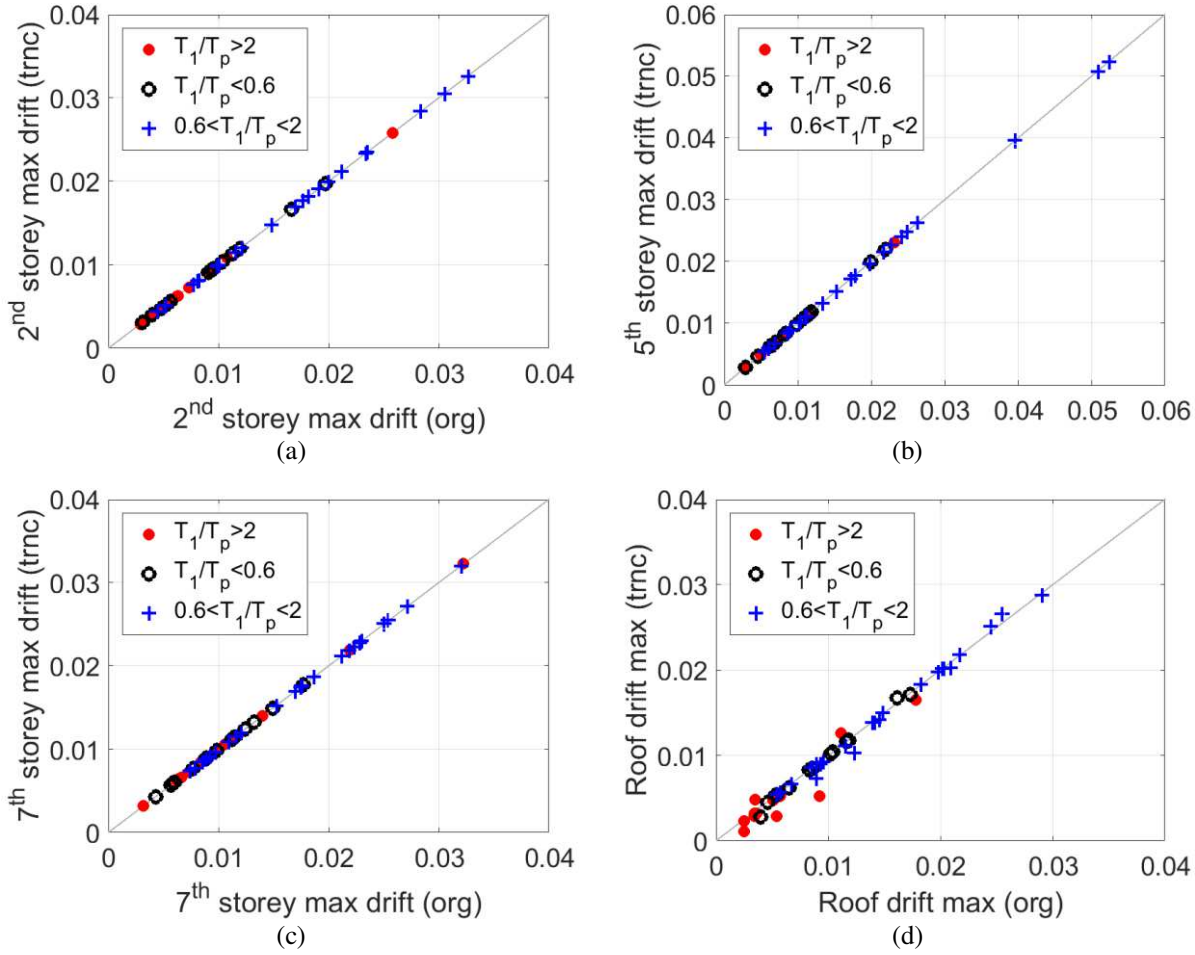

Figure 15: Maximum interstorey drift at different stories of the building, (a) 2nd Storey, (b) 5th Storey, (c) 7th storey and (d) 9th storey (roof).

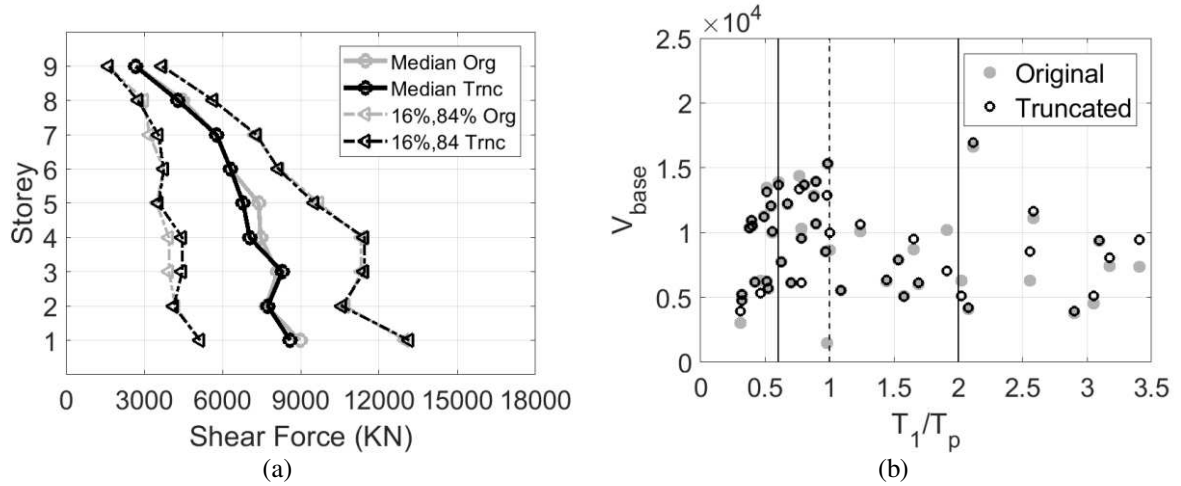

Figure 16: (a) Profiles of the maximum median storey shear force along with the standard deviation of storey shears. (b) Dispersion of the maximum base shear for original and truncated records versus T_1/T_p.

Figure 15 shows the maximum drift demand for the 2nd, the 5th, the 7th and the 9th (top) storey. The agreement is practically perfect for all stories with the exception of the top storey where some minor errors appear for ground motions with $T_1/T_p>2$. The maximum interstorey drifts occur mainly for records with T_1/T_p between 0.6 and 2, and in some cases for $T_1/T_p>2$, while for the structure considered, the peak values appear at the middle stories of the building.

Figure 16a shows the profiles of the median shear forces along the height of the building and the corresponding 16% and 84% percentiles. Very good agreement is again obtained, since the damage patterns are very close. Some minor differences are observed with respect to the demand in stories 3, 4 and 5. Furthermore, Figure 16b compares the base shear demand for the original and the truncated signal. It should be pointed out that the maximum values of the base shear are computed in the period range $0.5<T_1/T_p<1$, while (although not shown) most differences appear at the 1st and 5th storey, as also applies for the interstorey drifts (Figure 15).

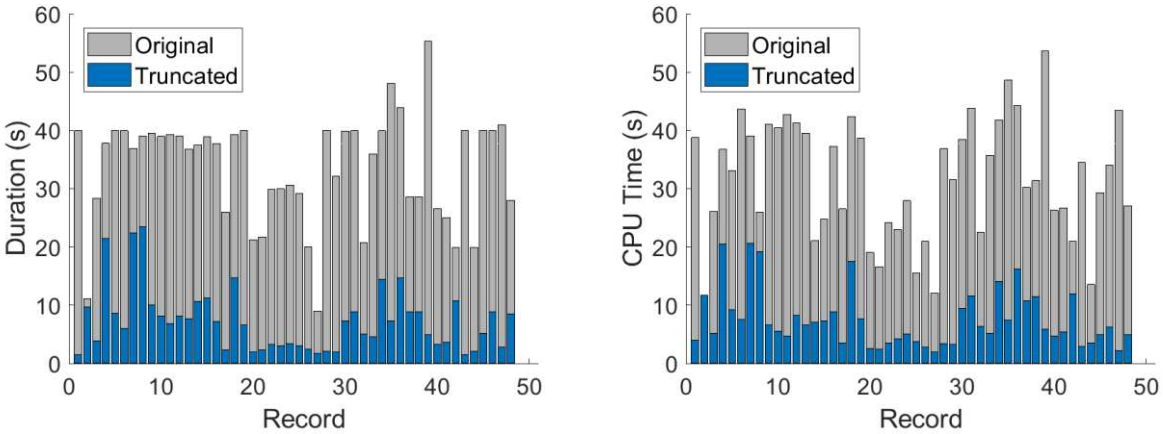

Figure 17: (a) comparison of the duration of the original ground motion and the corresponding truncated signal, and (b) CPU time required for the nonlinear response histories.

Figure 17 compares the duration of the truncated signal with that of the original ground motion. The plots prove that the proposed wavelet-based truncation can be used to efficiently accelerate seismic performance assessment studies. Furthermore, Figure 17b shows the improved CPU run times, which also leads to reduced storage demand of the analyses output. It is therefore evident that the proposed record truncation can reduce considerably the simulation time with a minor loss of accuracy, also in the case of multi-degree-of-freedom systems.

CONCLUSIONS

The proposed record truncation approach can be used to considerably simplify the input signal and accelerate the seismic performance assessment, especially in the case of pulse-like ground motions. More specifically, the truncation procedure is efficient for records with a pulse index that exceeds 0.65 which is in agreement with the findings of Kardoutsou *et al.* (2017). A lower pulse index (PI<0.65) may also give accurate results, although this is not a priori guaranteed. Furthermore, the truncation does not require baseline correction and thus it can be integrated to give truncated realistic velocity and displacement time histories. The proposed approach has been validated through the study of different structural systems. Elastoplastic systems are first studied in order derive inelastic displacement and acceleration spectra. Subsequently, three single-degree-of-freedom oscillators with in-cycle and cyclic degradation are investigated. The effect of the proposed truncation approach is finally applied on a nine-storey steel building, the well-know LA9 building. Almost in all cases, the seismic demand, measured in terms of displacement, drift and shear forces, obtained using the truncated signal will produce close estimates within a fraction of the CPU time required when the original complete record is used.

REFERENCES

Arias A (1970) A measure of earthquake intensity. In: Hansen RJ (ed) Seismic design for nuclear power plants. MIT Press, pp 438-483.

Baker JW (2007) Quantitative classification of near-fault ground motions using wavelet analysis. Bulletin of the Seismological Society of America 97: 1486-1501.

Baker JW, Cornell CA (2008) Vector-valued intensity measures for pulse-like near-fault ground motions. Engineering Structures 30: 1048–1057.

Bertero VV, Mahin SA, Herrera RA (1978) A seismic design implication of near-fault San Fernando earthquake records. Earthquake Engineering and Structural Dynamics 6: 31–42.

Bolt BA (1973) Duration of strong ground motion. In: Proceedings of the 5th World Conference on Earthquake Engineering Vol. 1, pp 1304-1313.

Bommer JJ & Martinez-Pereira A (1996) The prediction of strong ground motion duration for engineering design. In: Proceedings of the 11th World Conference on Earthquake Engineering Vol. 84, Acapulco, Mexico, pp 23-28.

Bommer JJ & Martinez-Pereira A (2000) Strong ground motion parameters: definition, usefulness and predictability. In: Proceedings of the 12th World Conference on Earthquake Engineering, Auckland, New Zealand.

Chopra AK, Chintanapakdee C (2001) Comparing response of SDF systems to near-fault and far-fault earthquake motions in the context of spectral regions. Earthquake Engineering and Structural Dynamics 30: 1769-1789.

Dimakopoulou V, Fragiadakis M, Spyrakos CC (2013) Influence of modeling parameters on the response of degrading systems to near-field ground motions. Engineering Structures 53:10–24.

FEMA P-695 Quantification of Building Seismic Performance Factors and commentary for the seismic rehabilitation of buildings, FEMA P-695 Report, prepared by the Applied Technology Council for the Federal Emergency Management Agency (2009), Washington DC.

Gupta A and Krawinkler H (1999) Seismic Demands for Performance Evaluation of Steel Moment Resisting Frame Structures. In: John A. Blume Earthquake Engineering Center Report No. 132, Department of Civil Engineering, Stanford University.

Husid R (1969) Caracteristicas de terremotos. Analisis general, Revista IDIEM 8(1): 21-42.

Iervolino I, Chioccarelli E, Baltzopoulos G (2012) Inelastic displacement ratio of near-source pulse-like ground motions, Short Communication. https://doi.org/10.1002/eqe.2167.

Jin A-Y, Pan J-W, Wang J-T, & Du X-L, (2020) A spectrum-based earthquake record truncation method for nonlinear dynamic analysis of arch dams. Soil Dynamics and Earthquake Engineering, 132, 106104. https://doi.org/10.1016/j.soildyn.2020.106104.

Kardoutsou V, Taflampas I & Psycharis IN (2017) A new pulse indicator for the classification of ground motions. Bulletin of the Seismological Society of America, 107(3):1356-1364.

Khaloo A, Nozhati S, Masoomi H, Faghihmaleki H (2016). Influence of earthquake record truncation on fragility curves of RC frames with different damage indices. J Build Eng 7: 23–30.

Mavroeidis GP and Papageorgiou AS (2003) A Mathematical Representation of Near-Fault Ground Motions. Bulletin of the Seismological Society of America 93(3):1099-1131.

McKenna F and Fenves GL (2001) The OpenSees Command Language Manual-Version 1.2, Pacific Earthquake Engineering Research Centre, University of California.

Mimoglou P, Psycharis IN & Taflampas IM (2014) Explicit determination of the pulse inherent in pulse-like ground motions. Earthquake Engineering & Structural Dynamics 43(15): 2261-2281.

Newmark NM, Hall WJ (1982) Earthquake Spectra and Design, Earthquake Engineering Research Center, University of California.

Peer-Pacific Earthquake Engineering Research Center (2013). Strong motion database. http://peer.berkeley.edu/peer_ground_motion_database. Accessed July 2013.

Repapis CC, Mimoglou PP, Dimakopoulou VV, Psycharis IN Taflampas IM (2020) Efficient strong ground motion duration of pulse-like records for nonlinear structural analyses, Earthquake Engineering and Structural Dynamics 2020: 1-19.

Riddell R (2007) On ground motion intensity indices. Earthquake Spectra 23(1):147-173.

Ruiz-García J (2011) Inelastic Displacement Ratios for Seismic Assessment of Structures Subjected to Forward-Directivity Near-Fault Ground Motions. Journal of Earthquake Engineering 15: 449-468.

Ruiz-García J, Miranda E (2007) Probabilistic Estimation of maximum inelastic displacement demands for performance-based design. Earthquake Engineering & Structural Dynamics 36: 1235-1254.

Sarma SK (1971) Energy flux of strong earthquakes. Tectonophysics 11(3): 159-173.

Spyrakos CC, Maniatakis ChA, Taflambas J (2008) Evaluation of near source seismic records based on damage potential parameters. Case study: Greece. Soil Dynamics & Earthquake Engineering 28: 738-753.

Srivastav S, Nau JM (1988) Structural response to truncated earthquake accelerograms. J Struct Eng 114(5): 1189–92.

Taflambas IM, Maniatakis ChA, Spyrakos CC (2008) Estimation of input seismic energy by means of a new definition of strong ground motion duration. In: 14th World Conference on Earthquake Engineering, Beijing, China, Report No. S10-065, 12, Vol. 17.

Trifunac MD & Brady AG (1975) A study on the duration of strong earthquake ground motion. Bulletin of the Seismological Society of America 65(3): 581-626.

APPENDIX

Table 2: The 48 near-fault records adopted.

#	Year	NGA	Tp(s)	Event/ Station	A(cm/s)	γ	v(o)	td(s)	Total Duration	Proposed Duration
1	1979	150	0.94	Coyote Lake / Gilroy Array #6	44.94	1.6	355	1.93	27.08	1.46
2	1979	158	1.64	Imperial Valley-06 / Aeropuerto Mexicali	46.78	2.1	345	3.64	11.14	9.68
3	1979	159	1.90	Imperial Valley-06 / Agrarias	44.04	2.0	25	5.87	28.35	3.79
4	1979	161	4.78	Imperial Valley-06 / Brawley Airport	43.38	1.8	135	2.67	37.77	21.40
5	1979	170	4.78	Imperial Valley-06 / EC County Center FF	43.38	1.8	135	2.67	39.96	8.60
6	1979	171	3.01	Imperial Valley-06 / EC County Center FF	114.85	1.4	0	2.86	39.96	5.99
7	1979	173	6.08	Imperial Valley-06/ El Centro Array #10	58.79	1.1	140	3.66	36.95	22.41
8	1979	174	6.39	Imperial Valley-06/ El Centro Array #11	8.55	2.9	245	0.60	38.99	23.47
9	1979	178	5.55	Imperial Valley-06/ El Centro Array #3	39.65	1.2	180	5.00	36.93	9.98
10	1979	179	4.32	Imperial Valley-06/ El Centro Array #4	71.39	1.9	125	2.00	38.95	8.16
11	1979	180	3.79	Imperial Valley-06 / El Centro Array #5	86.02	1.8	135	3.37	39.24	6.76
12	1979	181	3.94	Imperial Valley-06 / El Centro Array #6	97.49	1.9	85	2.62	39.01	8.16
13	1979	182	3.44	Imperial Valley-06 / El Centro Array #7	74.50	2.2	45	2.52	36.79	7.67
14	1979	183	5.08	Imperial Valley-06 / El Centro Array #8	69.50	1.1	80	3.37	37.53	10.64
15	1979	184	5.86	Imperial Valley-06/El Centro Differential Array	60.43	1.1	70	2.66	38.93	11.20
16	1979	185	4.24	Imperial Valley-06/El Centro Holtville Post Office	47.52	1.7	175	3.35	37.72	7.20
17	1980	250	1.14	Mamoth Lakes-06 / Long Valley (Upr L Abut)	34.99	1.4	300	4.59	25.93	2.25
18	1980	292	2.64	Irpinia-Italy-01 / Sturno	23.95	5.6	110	1.13	39.31	14.72
19	1981	316	3.00	Westmorland /Parachute Test Site	25.91	2.2	300	7.54	39.97	6.59
20	1983	407	0.56	Coalinga-05 / Oil City	35.39	3.4	0	2.22	21.21	1.91
21	1983	415	0.75	Coalinga-05 / Transmitter Hill	44.06	1.5	135	2.54	21.74	2.29
22	1984	451	0.77	Morgan Hill / Coyote Lake Dam (SW Abut)	42.78	4.2	300	2.30	29.93	3.26
23	1984	459	1.17	Morgan Hill / Gilroy Array #6	31.87	2.6	235	4.45	29.96	3.01
24	1986	503	1.49	Taiwan SMART1(40) / SMART1 C00	29.00	2.1	215	5.91	30.59	3.42
25	1986	508	1.39	Taiwan SMART1(40) / SMART1 M07	35.07	2.1	215	10.29	29.12	3.05
26	1986	529	1.44	N. Palm Springs / North Palm Springs	56.48	1.5	345	1.80	20.00	2.41
27	1986	568	0.70	San Salvador / Geotech Investig Center	68.43	2.2	190	0.63	9.00	1.71
28	1987	615	0.81	Whittier Narrows-01 / Downey - Co Maint Bldg	27.35	2.5	260	4.36	39.97	2.01
29	1987	645	0.78	Whittier Narrows-01 / LB - Orange Ave	30.64	2.4	255	5.10	32.08	1.91
30	1989	766	1.54	Loma Prieta / Gilroy Array #2	28.64	4.8	270	1.16	39.92	7.34
31	1989	802	6.48	Loma Prieta / Saratoga - Aloha Ave	36.31	1.2	180	3.10	39.93	8.79
32	1992	821	2.42	Erzincan-Turkey / Erzincan	89.81	1.7	20	1.58	20.75	5.08
33	1992	828	2.74	Cape Mendocino / Petrolia	57.86	1.5	325	1.13	35.98	4.55
34	1992	838	7.57	Landers / Barstow	22.79	1.7	135	11.2	39.94	14.40
35	1992	879	4.57	Landers / Lucerne	96.72	1.6	65	7.03	48.10	7.29
36	1992	900	7.33	Landers / Yermo Fire Station	39.16	2.0	175	10.95	43.95	14.65
37	1994	982	2.94	Northridge-01 / Jensen Filter Plant	60.02	3.0	285	0.00	28.59	8.78
38	1994	983	2.94	Northridge-01 / Jensen Filter Plant Generator	60.02	3.0	285	0.00	28.59	8.78
39	1994	1009	2.35	Northridge-01 / LA-Wadsworth VA Hospital North	41.98	1.1	110	8.16	55.32	4.91
40	1994	1013	2.17	Northridge-01 / LA-Dam	76.26	1.1	220	1.78	26.55	3.23
41	1994	1045	2.39	Northridge-01 / Newhall-W Pico Canyon Rd.	117.85	1.2	290	3.82	24.98	3.56

42	1994	1050	3.37	Northridge-01 / Pacoima Dam (downstream).	11.71	3.2	25	0.04	19.96	10.71
43	1994	1051	0.90	Northridge-01 / Pacoima Dam (upper left)	100.31	1.6	255	3.26	39.94	1.44
45	1994	1063	1.11	Northridge-01/ Rinaldi Receiving Station	132.51	1.9	240	1.55	19.90	2.10
45	1994	1085	3.06	Northridge-01/Sylmar Converter Station East	89.17	1.6	175	1.15	39.97	5.20
46	1994	1086	2.56	Northridge-01/Sylmar Olive View Med FF	61.88	3.6	355	0.37	39.98	8.90
47	1995	1119	1.23	Kobe, Japan / Takarazuka	55.97	2.3	145	3.82	40.95	2.82
48	1999	1161	4.88	Kocaeli, Turkey / Gebze	42.18	1.8	190	3.37	27.98	8.49

T_p (sec): The period of the harmonic oscillation of the wavelet.
A (cm/sec): The amplitude of the wavelet.
γ: The duration of the wavelet, which measures the number of the oscillations.
v (^{o}): Phase shift.
t_d (sec): Time delay for the initiation of the pulse.

Figures

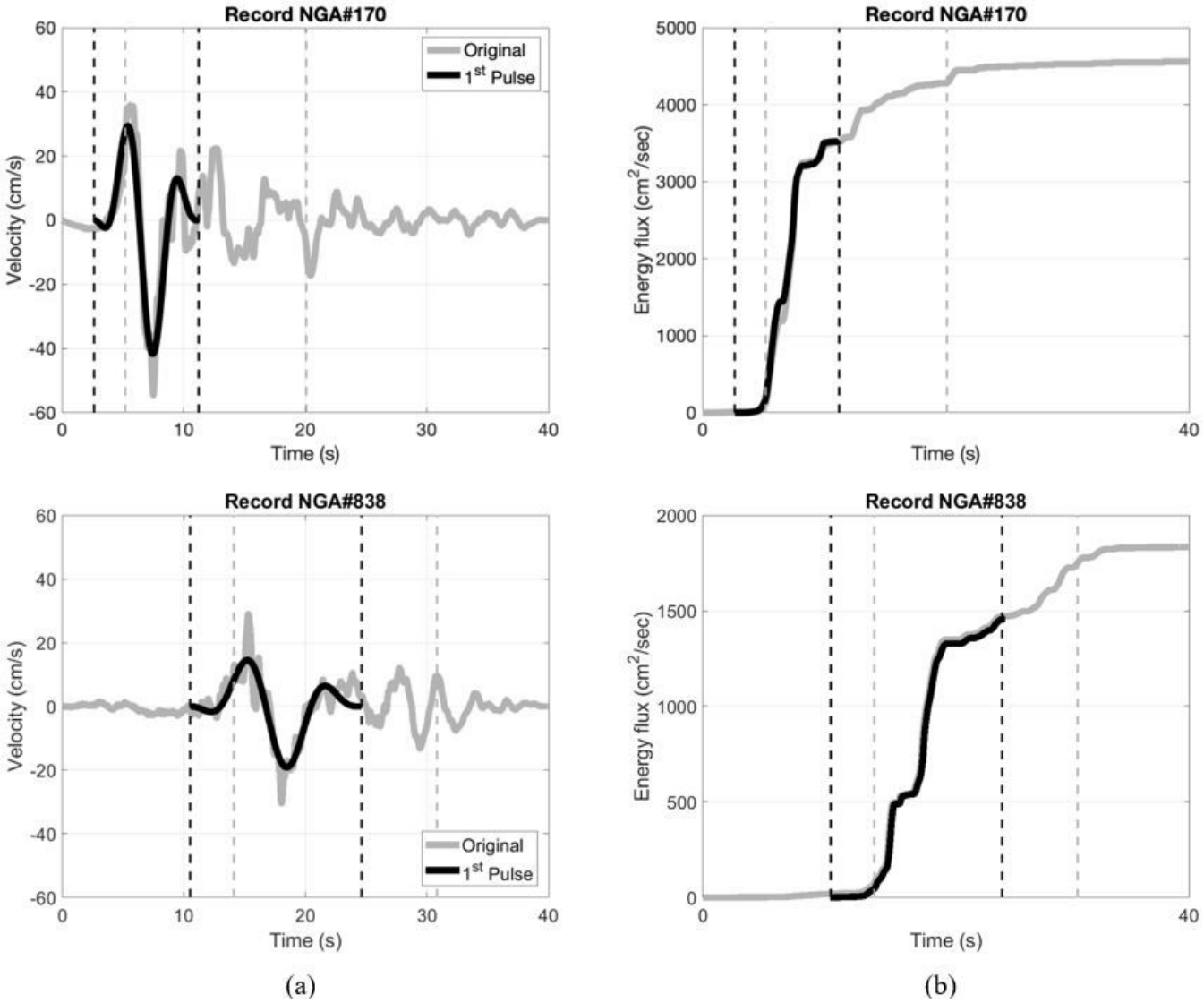

Figure 1

(a) Velocity time history showing the total, the proposed wavelet-based and the significant duration definition, (b) Energy flux (records NGA #170 and NGA #838).

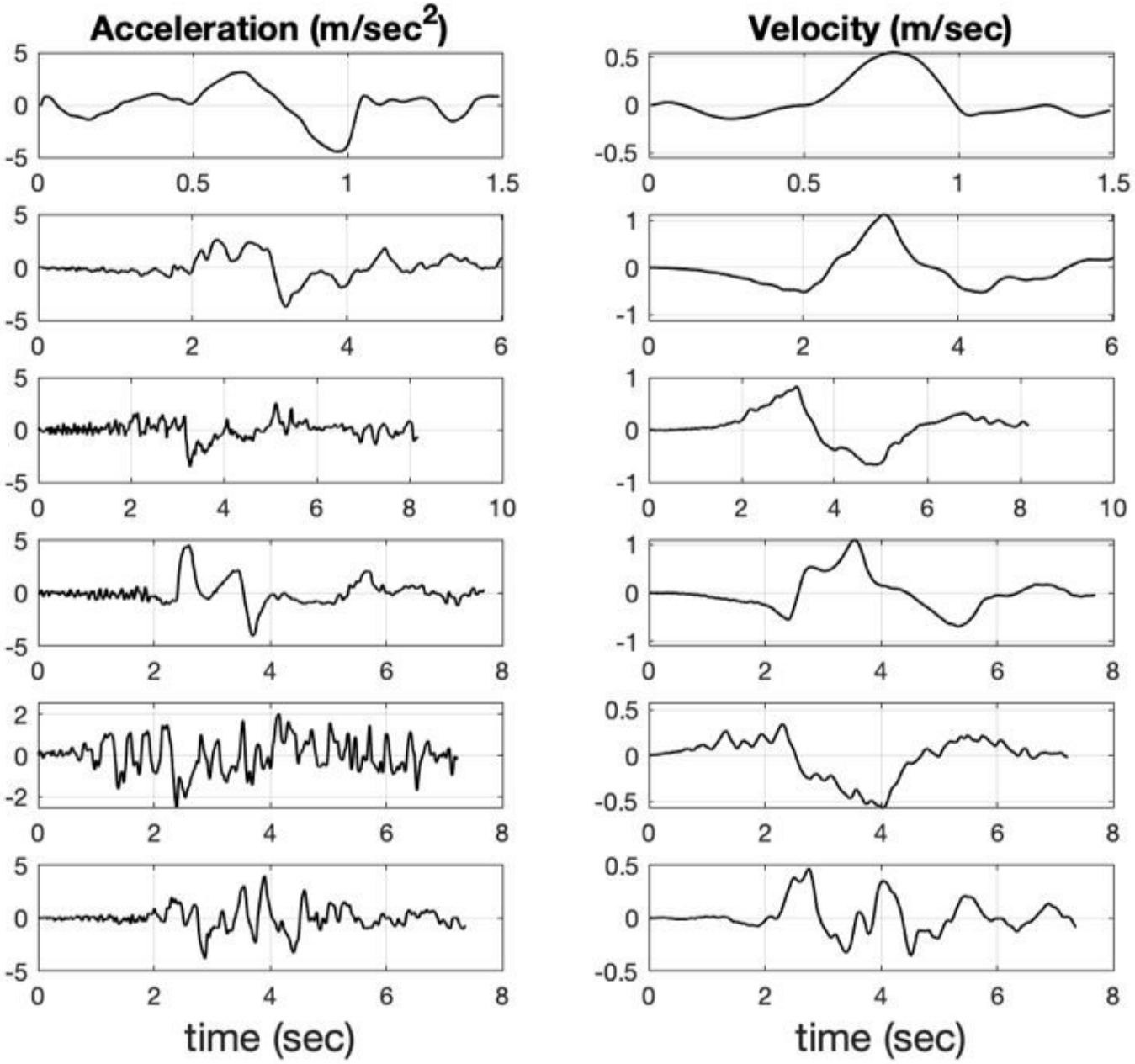

Figure 2

Acceleration and velocity time histories of truncated signals.

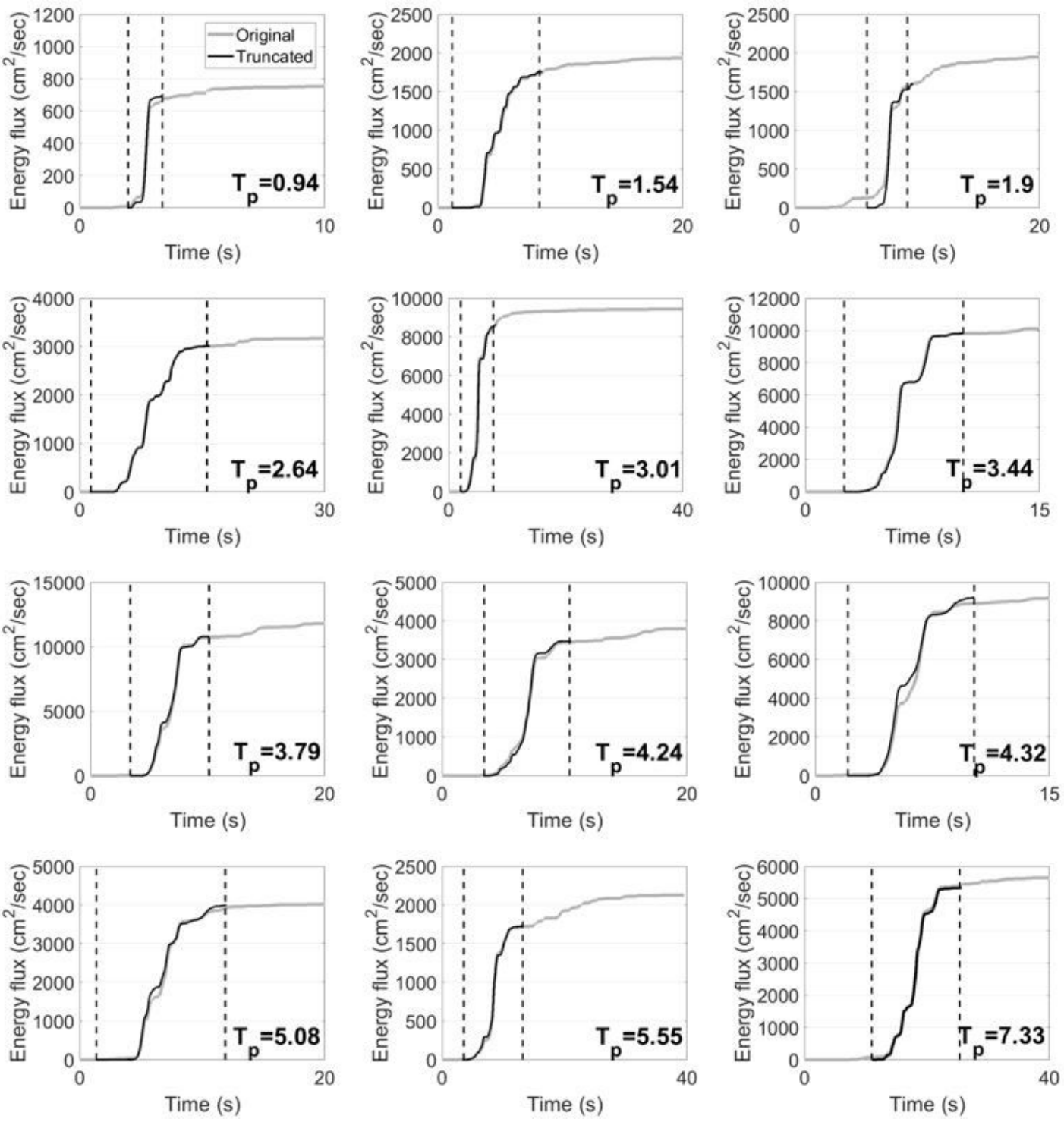

Figure 3

Energy flux and proposed wavelet-based duration for twelve ground motions.

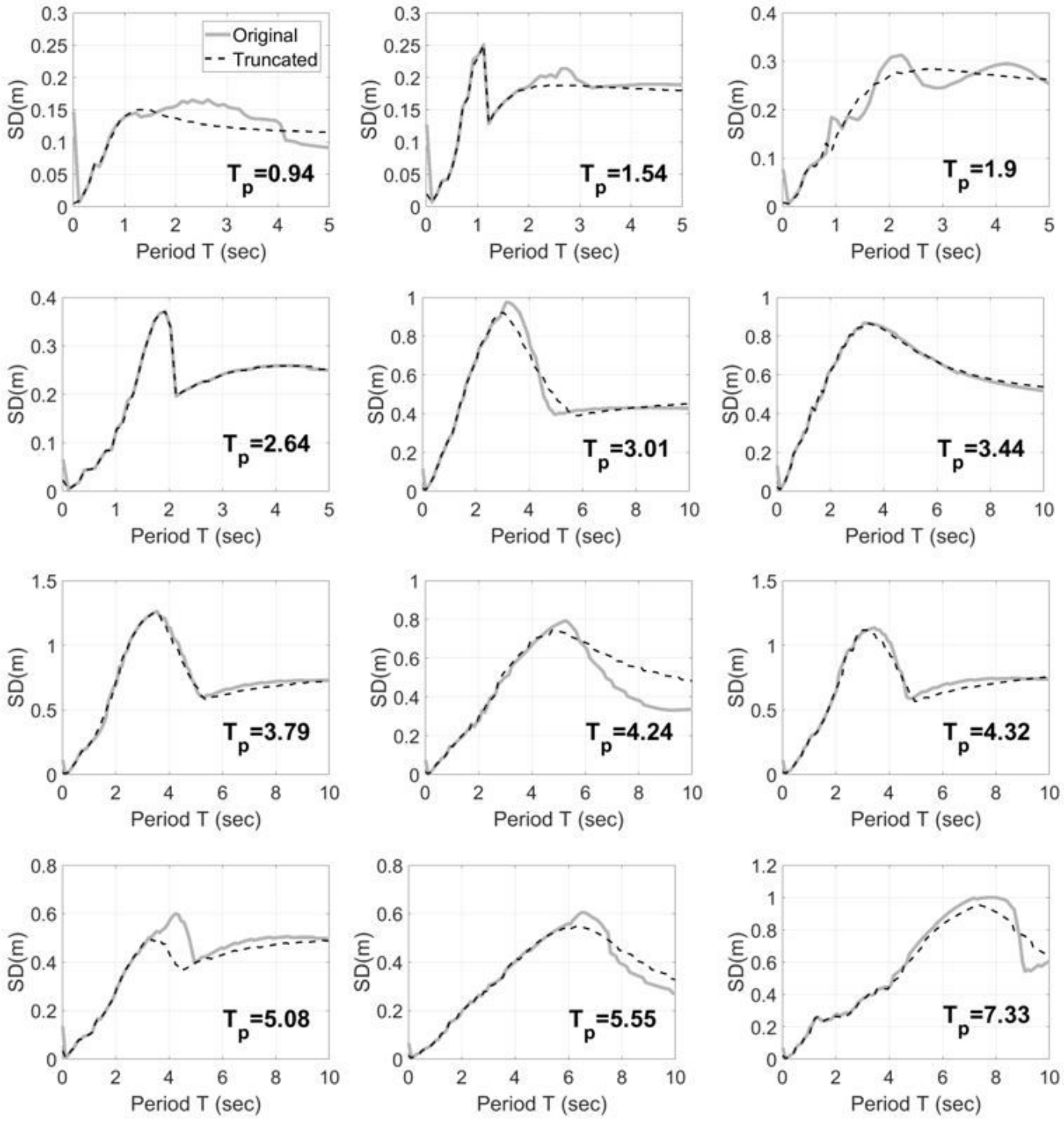

Figure 4

Displacement spectra with constant ductility μ=6.

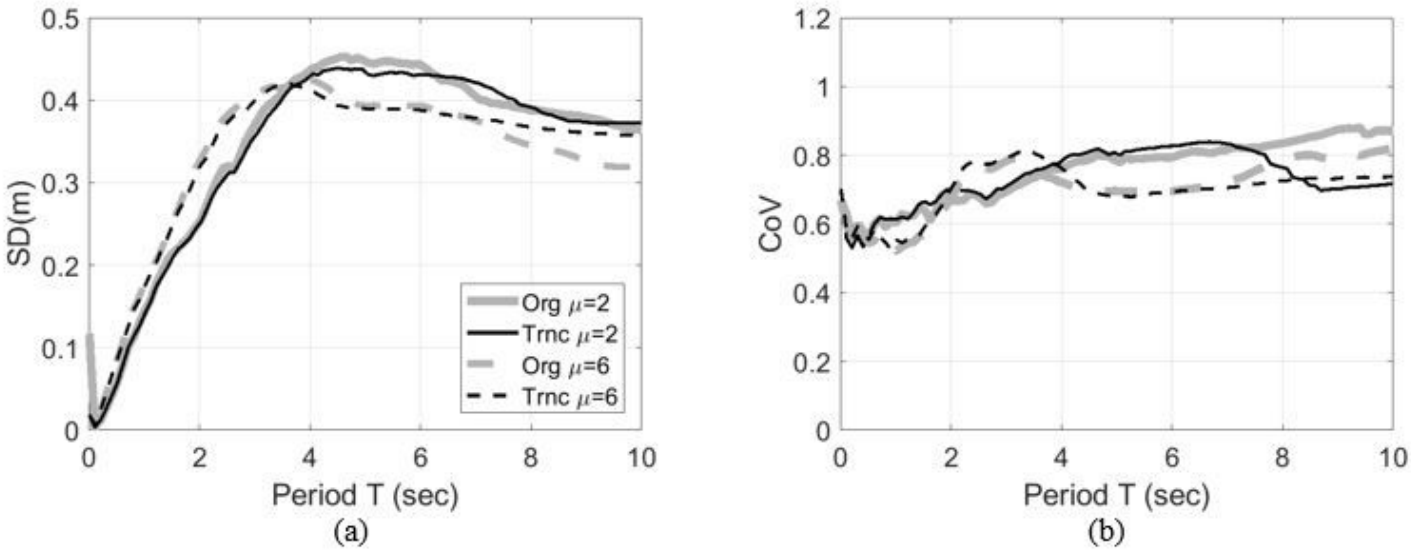

Figure 5

(a) Mean inelastic displacement spectra, (b) coefficient of variation of inelastic displacement spectra, calculated for constant ductility μ factor equal to μ=2 (solid line) and μ=6 (dashed line).

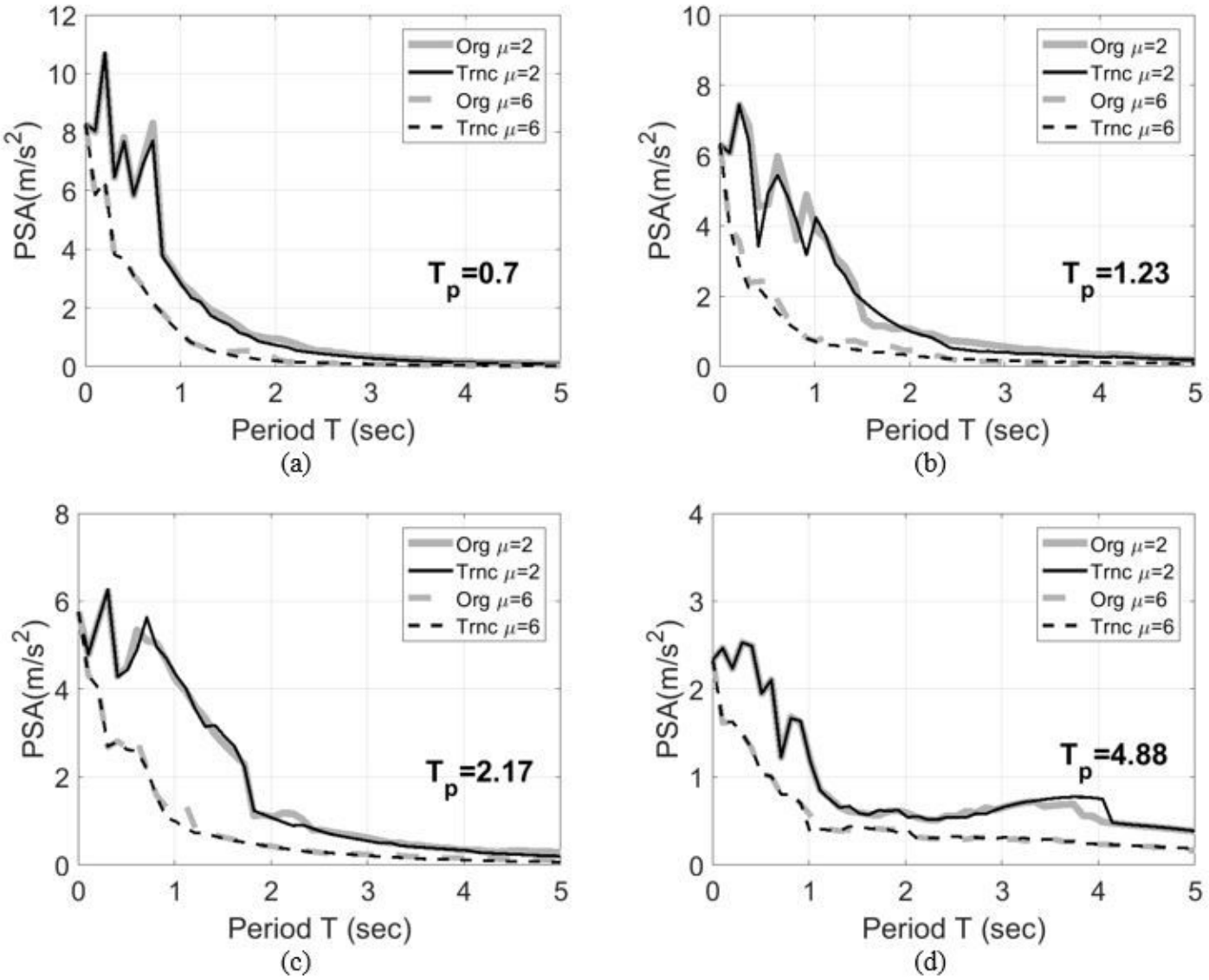

Figure 6

Constant ductility acceleration spectra (μ=2, 6): (a) NGA#568, (b) NGA#1119, (c) NGA#1013, (d) NGA#1161.

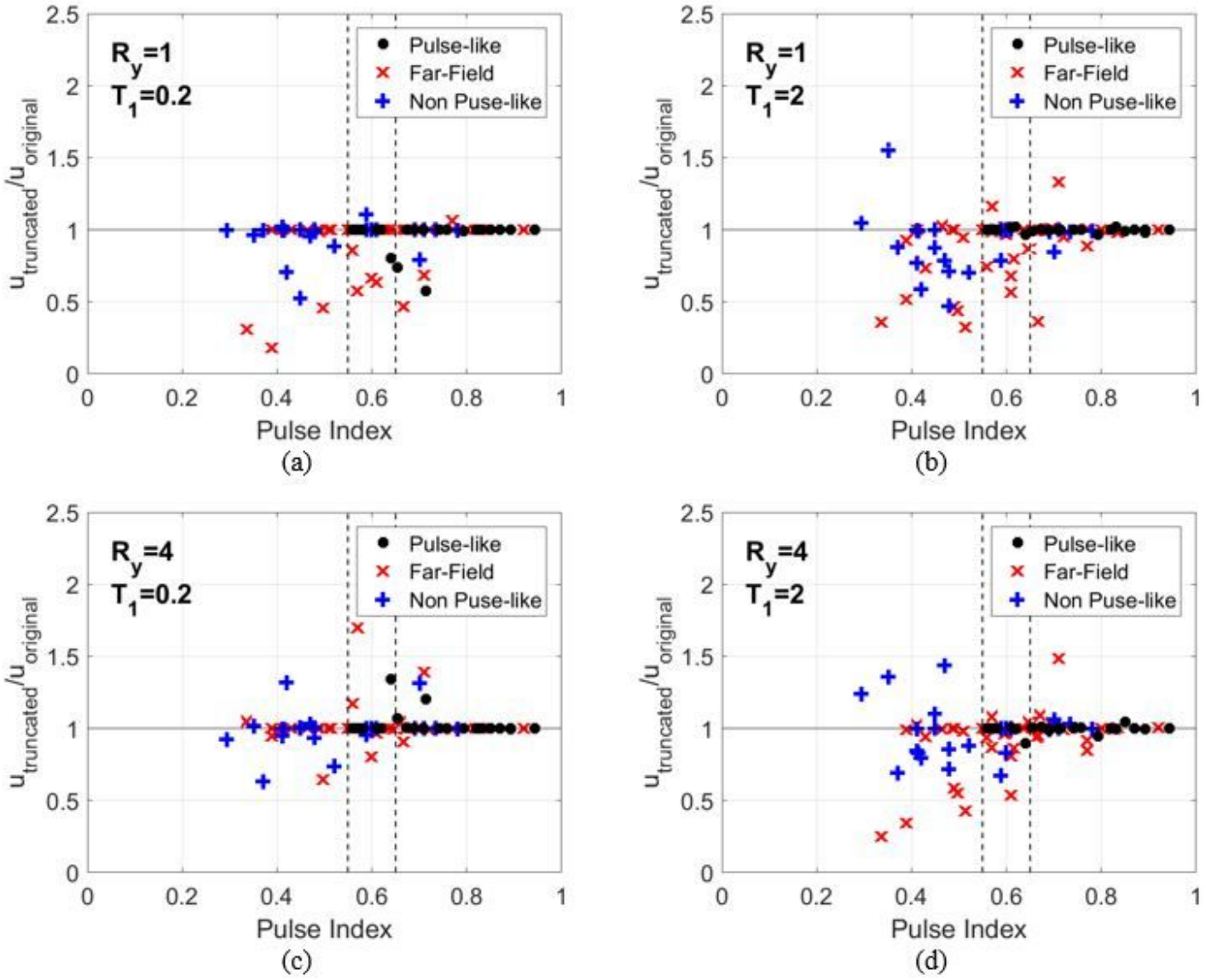

Figure 7

Ratio of the maximum top displacement of elastoplastic SDOF systems computed for the original and truncated record versus the corresponding pulse index for elastoplastic systems with: (a) Ry=1, T1=0.2sec, (b) Ry=1, T1=2sec, (c) Ry=4, T1=0.2sec, and (d) Ry=4, T1=2sec.

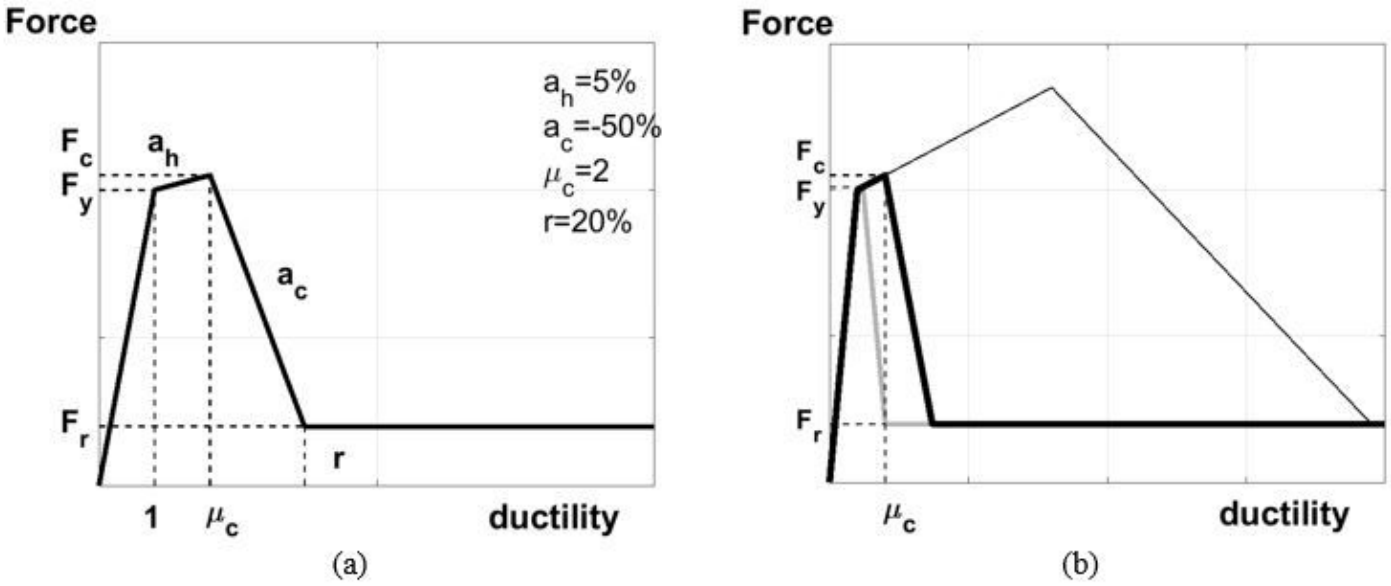

Figure 8

(a) Reference oscillator, (b) brittle oscillator (light grey line), ductile oscillator (black thin line) and reference oscillator (black line).

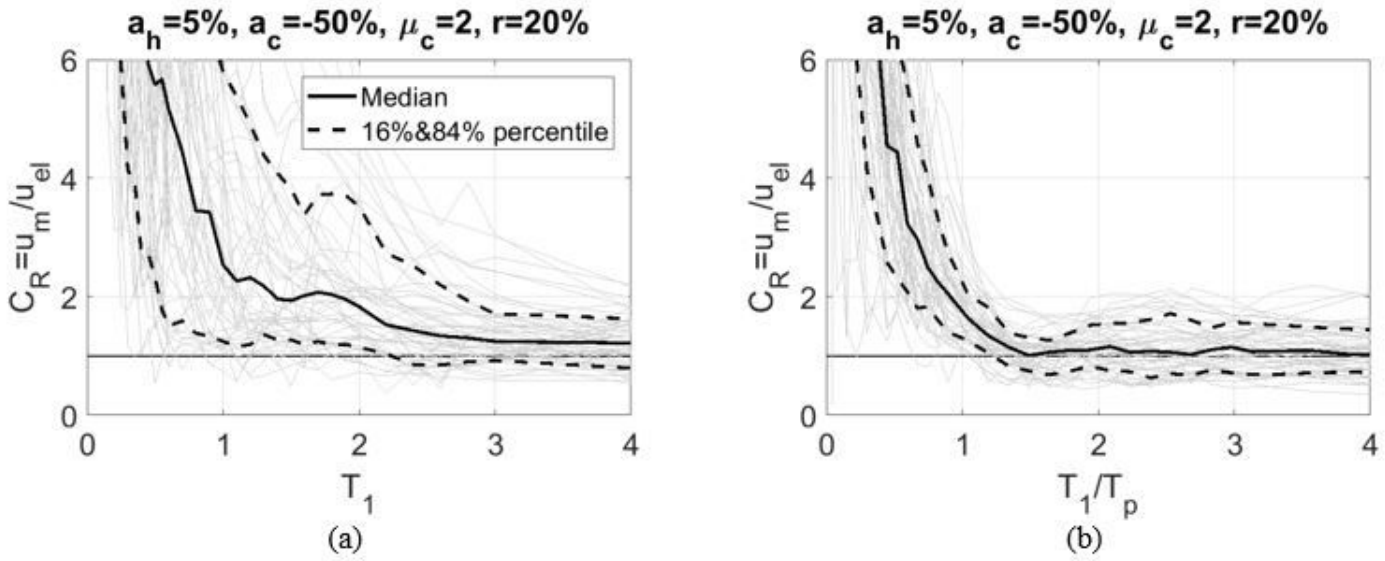

Figure 9

Reference oscillator (Ry=6) under original ground motions: CR ratio values versus (a) oscillator period T1, (b) oscillator period normalized with the pulse period T1/Tp.

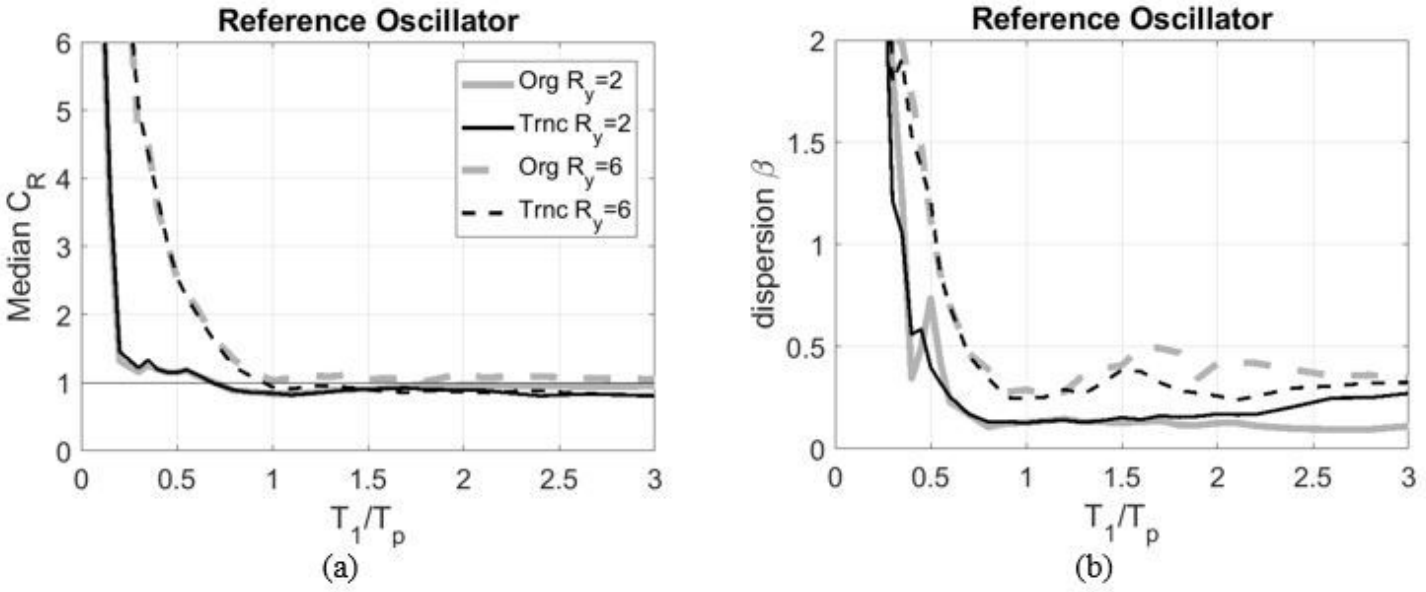

Figure 10

(a) Median CR of the reference degrading SDOF oscillator subjected to the original ground motion and the corresponding truncated signal for Ry=2 and Ry=6, (b) dispersion β of CR, calculated for Ry=2 and Ry=6.

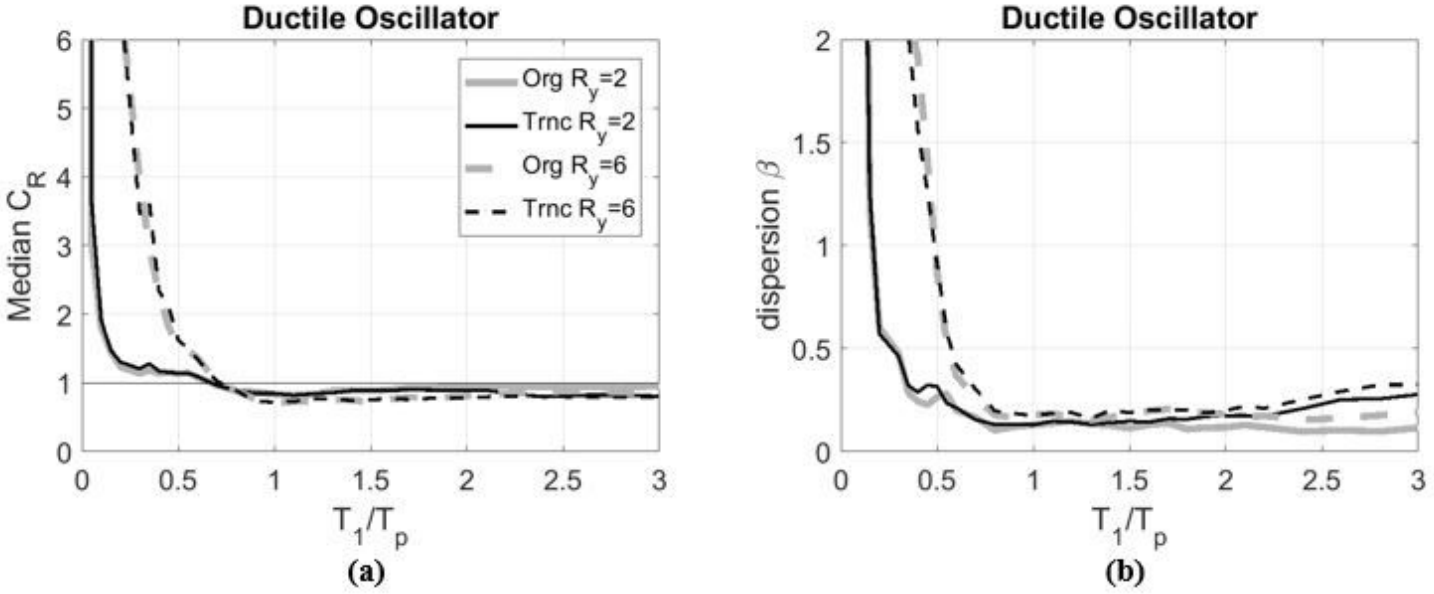

Figure 12

Median CR of the ductile oscillator subjected to the original ground motion and the corresponding truncated signal for Ry=2 and Ry=6, (b) dispersion β of CR, calculated for Ry=2 and Ry=6.

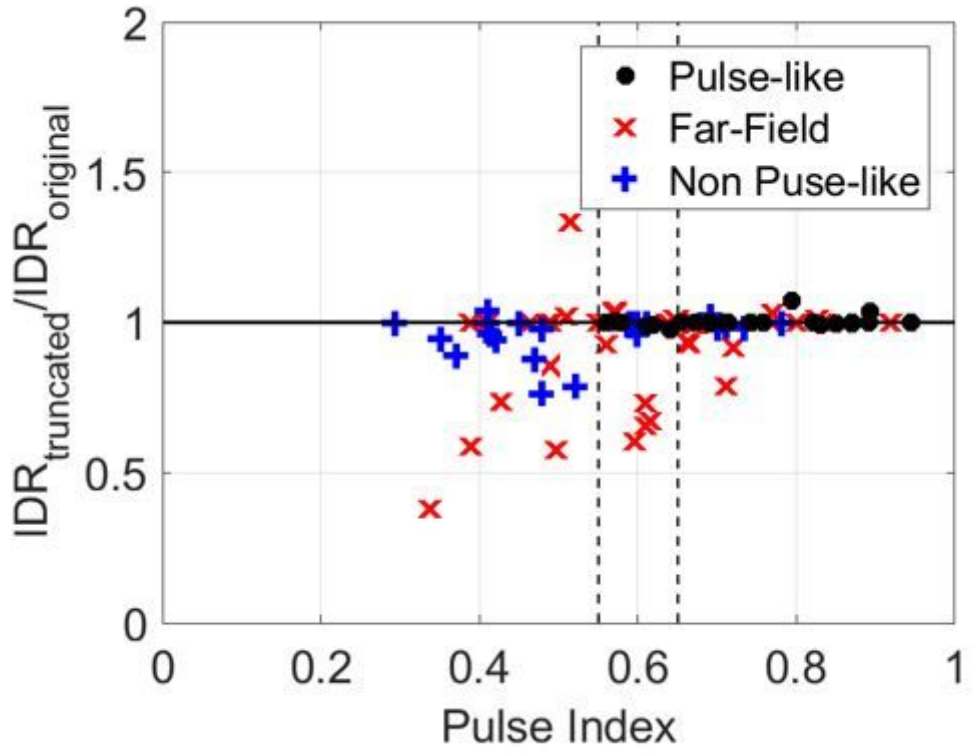

Figure 13

Ratio of the maximum interstorey drift for the 9-storey steel moment frame versus the calculated cross correlation.

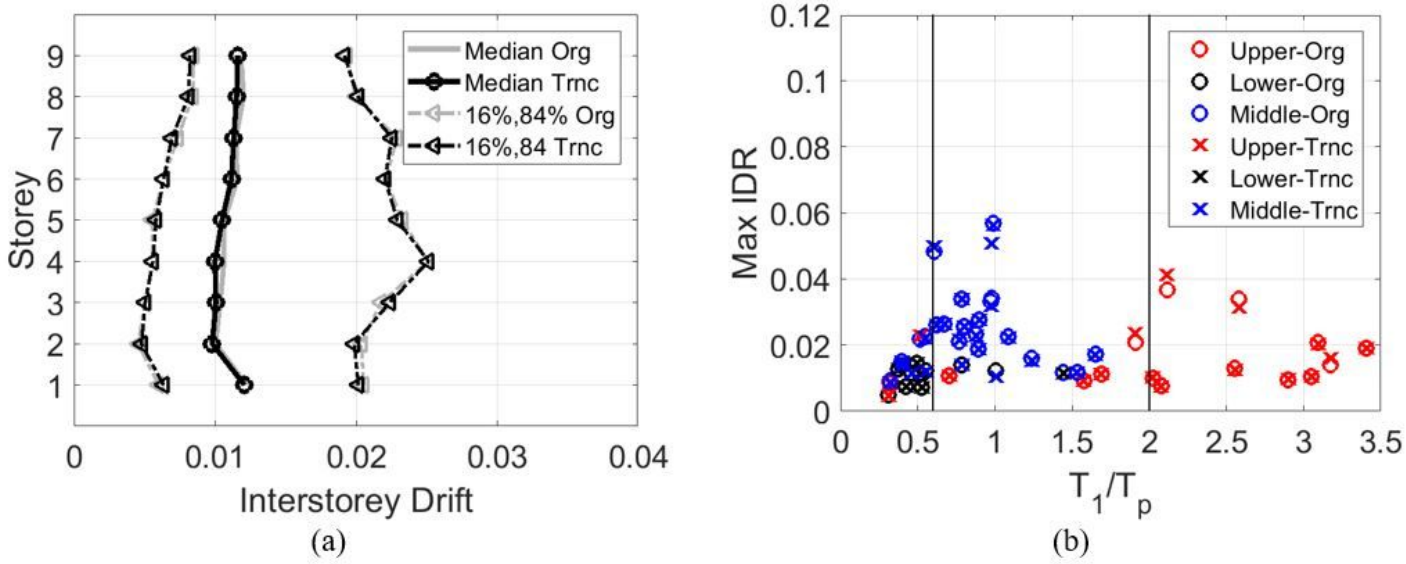

Figure 14

(a) Profile of the median and the 16 and 84% percentiles drift demand for the 48 pulse-type ground motions; (b) Maximum interstorey drift obtained using the original and the truncated records versus the T1/Tp ratio

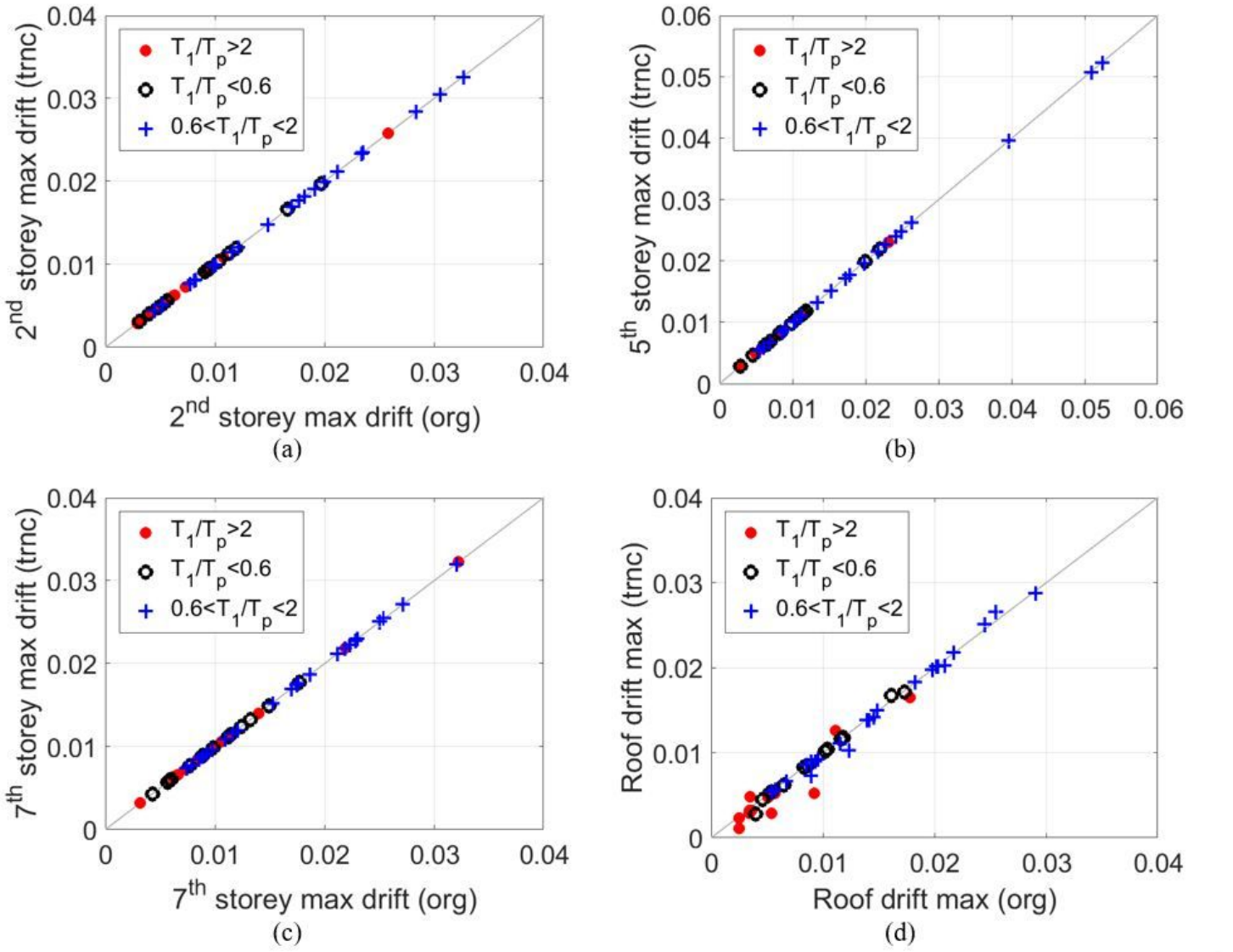

Figure 15

Maximum interstorey drift at different stories of the building, (a) 2nd Storey, (b) 5th Storey, (c) 7th storey and (d) 9th storey (roof).

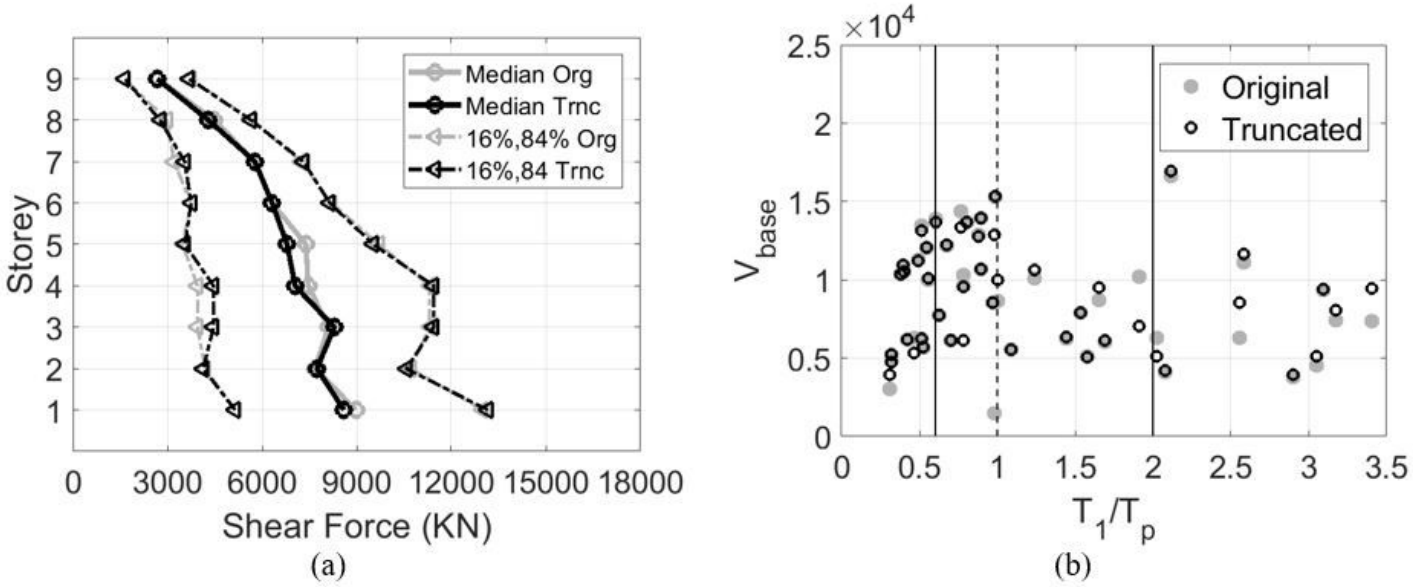

Figure 16

(a) Profiles of the maximum median storey shear force along with the standard deviation of storey shears. (b) Dispersion of the maximum base shear for original and truncated records versus T1/Tp.

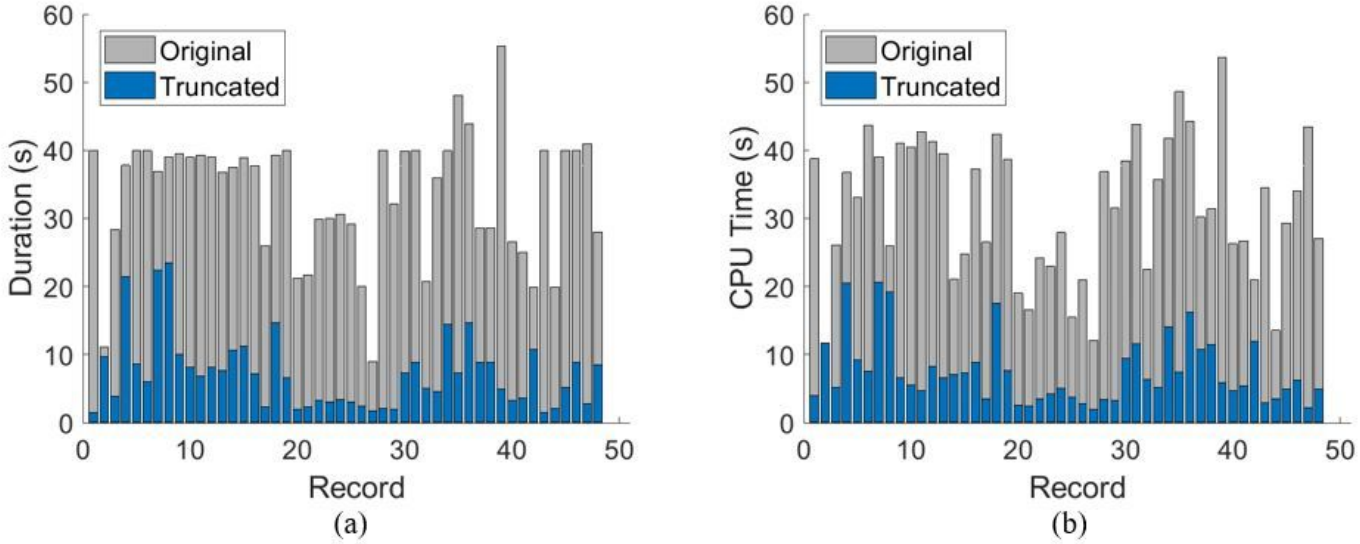

Figure 17

(a) comparison of the duration of the original ground motion and the corresponding truncated signal, and (b) CPU time required for the nonlinear response histories.

Supplementary Files

This is a list of supplementary files associated with this preprint. Click to download.

- Appendix.docx